
DiffWire: Inductive Graph Rewiring via the Lovász Bound

Anonymous Author(s)

Anonymous Affiliation

Anonymous Email

Abstract

Graph Neural Networks (GNNs) have been shown to achieve competitive results to tackle graph-related tasks, such as node and graph classification, link prediction and node and graph clustering in a variety of domains. Most GNNs use a message passing framework and hence are called MPNNs. Despite their promising results, MPNNs have been reported to suffer from over-smoothing, over-squashing and under-reaching. Graph rewiring and graph pooling have been proposed in the literature as solutions to address these limitations. However, most state-of-the-art graph rewiring methods fail to preserve the global topology of the graph, are neither differentiable nor inductive, and require the tuning of hyper-parameters. In this paper, we propose DIFFWIRE, a novel framework for graph rewiring in MPNNs that is principled, fully differentiable and parameter-free by leveraging the Lovász bound. Our approach provides a unified theory for graph rewiring by proposing two new, complementary layers in MPNNs: CT-LAYER, a layer that learns the commute times and uses them as a relevance function for edge re-weighting; and GAP-LAYER, a layer to optimize the spectral gap, depending on the nature of the network and the task at hand. We empirically validate the value of each of these layers separately with benchmark datasets for graph classification. DIFFWIRE brings together the learnability of commute times to related definitions of curvature, opening the door to creating more expressive MPNNs.

1 Introduction

Graph Neural Networks (GNNs) [1, 2] are a class of deep learning models applied to graph structured data. They have been shown to achieve state-of-the-art results in many graph-related tasks, such as node and graph classification [3, 4], link prediction [5] and node and graph clustering [6, 7], and in a variety of domains, including image or molecular structure classification, recommender systems and social influence prediction [8].

Most GNNs use a message passing framework and thus are referred to as Message Passing Neural Networks (MPNNs) [4]. In these networks, every node in each layer receives a message from its adjacent neighbors. All the incoming messages at each node are then aggregated and used to update the node’s representation via a learnable non-linear function –which is typically implemented by means of a neural network. The final node representations (called node embeddings) are used to perform the graph-related task at hand (e.g. graph classification). MPNNs are extensible, simple and have proven to yield competitive empirical results. Examples of MPNNs include GCN [3], GAT [9], GATv2 [10], GIN [11] and GraphSAGE [12]. However, they typically use transductive learning, i.e. the model observes both the training and testing data during the training phase, which might limit their applicability to graph classification tasks.

However, MPNNs also have important limitations due to the inherent complexity of graphs. Despite such complexity, the literature has reported best results when MPNNs have a small number of layers, because networks with many layers tend to suffer from *over-smoothing* [13] and *over-squashing* [14]. However, these models fail to capture information that depends on the entire structure of the graph [15] and prevent the information flow to reach distant nodes. This phenomenon is called *under-reaching* [16] and occurs when the MPNN’s depth is smaller than the graph’s diameter.

43 *Over-smoothing* [8, 17–19] takes place when the embeddings of nodes that belong to different classes
 44 become indistinguishable. It tends to occur in MPNNs with many layers that are used to tackle short-
 45 range tasks, i.e. tasks where a node’s correct prediction mostly depends on its local neighborhood.
 46 Given this local dependency, it makes intuitive sense that adding layers to the network would not
 47 help the network’s performance.

48 Conversely, long-range tasks require as many layers in the network as the range of the interaction
 49 between the nodes. However, as the number of layers in the network increases, the number of
 50 nodes feeding into each of the node’s receptive field also increases exponentially, leading to *over-*
 51 *squashing* [14, 20]: the information flowing from the receptive field composed of many nodes is
 52 compressed in fixed-length node vectors, and hence the graph fails to correctly propagate the messages
 53 coming from distant nodes. Thus, over-squashing emerges due to the distortion of information flowing
 54 from distant nodes due to graph bottlenecks that emerge when the number of k -hop neighbors grows
 55 exponentially with k .

56 Graph pooling and *graph rewiring* have been proposed in the literature as solutions to address these
 57 limitations [14]. Given that the main infrastructure for message passing in MPNNs are the edges
 58 in the graph, and given that many of these edges might be noisy or inadequate for the downstream
 59 task [21], graph rewiring aims to identify such edges and edit them.

60 Many graph rewiring methods rely on edge sampling strategies: first, the edges are assigned new
 61 weights according to a *relevance function* and then they are re-sampled according to the new weights
 62 to retain the most relevant edges (i.e. those with larger weights). Edge relevance might be computed
 63 in different ways, including randomly [22], based on similarity [23] or on the edge’s curvature [20].

64 Due to the diversity of possible graphs and tasks to be performed with those graphs, optimal graph
 65 rewiring should include a *variety of strategies* that are suited not only to the task at hand but also to
 66 the nature and structure of the graph.

67 **Motivation.** State-of-the-art edge sampling strategies have three significant **limitations**. First,
 68 most of the proposed methods **fail to preserve the global topology of the graph**. Second, most
 69 graph rewiring methods are neither **differentiable** nor **inductive** [20]. Third, relevance functions that
 70 depend on a diffusion measure (typically in the spectral domain) are **not parameter-free**, which adds
 71 a layer of complexity in the models. In this paper, we address these three limitations.

72 **Contributions and outline.** The main contribution of our work is to propose a theoretical frame-
 73 work called DIFFWIRE for graph rewiring in MPNNs that is principled, fully differentiable, inductive,
 74 and parameter-free by leveraging the Lovász bound [15] given by Eq. 1. This bound is a mathematical
 75 expression of the relationship between the *commute times* (*effective resistance distance*) and the
 76 network’s *spectral gap*. *Inductive* means that given an unseen test graph, DIFFWIRE predicts the
 77 optimal graph structure for the task at hand without any parameter tuning. Given the recently reported
 78 connection between commute times and curvature [24], and between curvature and the spectral
 79 gap [20], our framework provides a unified theory linking these concepts. Our aim is to leverage
 80 diffusion and curvature theories to propose a new approach for graph rewiring that preserves the
 81 graph’s structure.

82 We first propose using the commute times as a relevance function for edge re-weighting. Moreover,
 83 we develop a differentiable, parameter-free layer in the GNN (CT-LAYER) to learn the commute
 84 times. Second, we propose an alternative graph rewiring approach by adding a layer in the network
 85 (GAP-LAYER) that optimizes the spectral gap according to the nature of the network and the task at
 86 hand. Finally, we empirically validate the proposed layers with state-of-the-art benchmark datasets in
 87 a graph classification task. We select a graph classification task to emphasize the inductive nature of
 88 DIFFWIRE: the layers in the GNN (CT-LAYER and GAP-LAYER) are trained to predict the CTs
 89 embedding and minimize the spectral gap for unseen graphs, respectively. This approach gives a great
 90 advantage when compared to SoTA methods that require optimizing the parameters of the models for
 91 each graph. CT-LAYER and GAP-LAYER learn the weights during training to predict the optimal
 92 changes in the topology of any unseen graph in test time.

93 The paper is organized as follows: Section 2 provides a summary of the most relevant related literature.
 94 Our core technical contribution is described in Section 3, followed by our experimental evaluation
 95 and discussion in Section 4. Finally, Section 5 is devoted to conclusions and an outline of our future
 96 lines of research.

97 2 Related Work

98 In this section we provide an overview of the most relevant works that have been proposed in the
 99 literature to tackle the challenges of over-smoothing, over-squashing and under-reaching in MPNNs
 100 by means of graph rewiring and pooling.

101 **Graph rewiring in MPNNs.** *Rewiring* is a process of changing the graph’s structure to control the
 102 information flow and hence improve the ability of the network to perform the task at hand (e.g. node
 103 or graph classification, link prediction...). Several approaches have been proposed in the literature for
 104 graph rewiring, such as connectivity diffusion [25] or evolution [20], adding new bridge-nodes [26]
 105 and multi-hop filters [27], and neighborhood [12], node [28] and edge [22] sampling.

106 Edge sampling methods sample the graph’s edges based on their weights or relevance, which might
 107 be computed in different ways. Rong et al. [22] show that randomly dropping edges during training
 108 improves the performance of GNNs. Klicpera et al. [25], define edge relevance according to the
 109 coefficients of a parameterized diffusion process over the graph. Then, the k -hop diffusion matrix
 110 is truncated to discard long-range interactions. For Kazi et al. [23], edge relevance is given by the
 111 similarity between the nodes’ attributes. In addition, a reinforcement learning process rewards edges
 112 leading to a correct classification and penalizes the rest.

113 Edge sampling-based rewiring has been proposed to tackle over-smoothing and over-squashing in
 114 MPNNs. Over-smoothing may be relieved by removing inter-class edges [29]. However, this strategy
 115 is only valid when the graph is homophilic, i.e. connected nodes tend to share similar attributes.
 116 Otherwise, removing these edges could lead to over-squashing [20] if their removal obstructs the
 117 message passing between distant nodes belonging to the same class (heterophily). Increasing the
 118 size of the bottlenecks of the graph via rewiring has been shown to improve node classification
 119 performance in heterophilic graphs, but not in homophilic graphs [20]. Recently, Topping et al. [20]
 120 propose an edge relevance function given by the edge curvature to mitigate over-squashing. They
 121 identify the bottleneck of the graph by computing the Ricci curvature of the edges. Next, they remove
 122 edges with high curvature and add edges around minimal curvature edges.

123 **Graph Structure Learning (GSL).** GSL methods [30] aim to learn an optimized graph structure and
 124 its corresponding representations *at the same time*. DIFFWIRE could be seen from the perspective of
 125 GSL: CT-LAYER, as a metric-based, neural approach, and GAP-LAYER, as a direct-neural approach
 126 to optimize the structure of the graph to the task at hand.

127 **Pooling in MPNNs.** In addition to graph rewiring, *pooling* layers simplify the original graph by
 128 compressing it into a smaller graph or a vector via pooling operators, which range from simple [31] to
 129 more sophisticated approaches, such as DiffPool [32] and MinCut pool [33]. Although graph pooling
 130 methods do not consider the edge representations, there is a clear relationship between pooling
 131 methods and rewiring since both of them try to reduce the flow of information through the graph’s
 132 bottleneck.

133 **Positional Encodings (PEs)** A Positional Encoding is a feature that describes the global or local
 134 position of the nodes in the graph. These features are related to random walk measures, the Laplacian’s
 135 eigenvectors [34] or commute time embeddings, as recently proposed by Velingker et al. [35].
 136 Positional Encodings are typically pre-computed and then used to build more expressive graph
 137 architectures, either by concatenating them to the node features or by building transformer models [36].
 138 Our work is related to PEs as CT-LAYER learns how to predict the PEs instead of pre-computing
 139 them. Thus, it may be seen as a method to automatically learn the PEs for graph rewiring.

140 3 Proposed Approach: DIFFWIRE for Inductive Graph Rewiring

141 DIFFWIRE provides a unified theory for graph rewiring by proposing two new, complementary layers
 142 in MPNNs: first, CT-LAYER, a layer that learns the commute times and uses them as a relevance
 143 function for edge re-weighting; and second, GAP-LAYER, a layer to optimize the spectral gap,
 144 depending on the nature of the network and the task at hand.

145 In this section, we present the theoretical foundations for the definitions of CT-LAYER and GAP-
 146 LAYER. First, we introduce the bound that our approach is based on: The Lovász bound. Table 2 in
 147 A.1 summarizes the notation used in the paper.

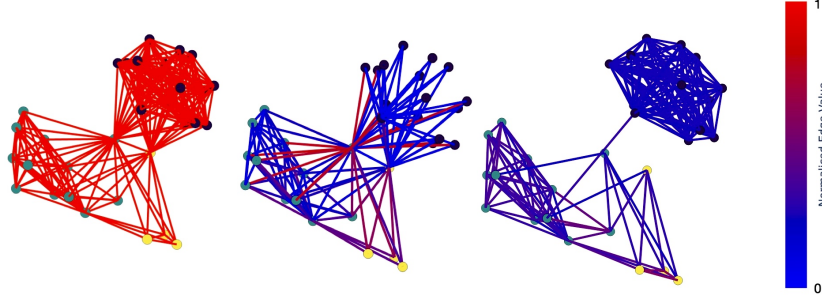


Figure 1: DIFFWIRE. Left: Original graph from COLLAB (test set). Center: Rewired graph after CT-LAYER. Right: Rewired graph after GAP-LAYER. Colors indicate the strength of the edges.

148 3.1 The Lovász Bound

149 The Lovász bound, given by Eq. 1, was derived by Lovász in [15] as a means of linking the spectrum
 150 governing a random walk in an undirected graph $G = (V, E)$ with the *hitting time* H_{uv} between any
 151 two nodes u and v of the graph. H_{uv} is the expected number of steps needed to reach (or hit) v from
 152 u ; H_{vu} is defined analogously. The sum of both hitting times between the two nodes, v and u , is the
 153 *commute time* $CT_{uv} = H_{uv} + H_{vu}$. Thus, CT_{uv} is the expected number of steps needed to hit v
 154 from u and go back to u . According to the Lovász bound:

$$\left| \frac{1}{\text{vol}(G)} CT_{uv} - \left(\frac{1}{d_u} + \frac{1}{d_v} \right) \right| \leq \frac{1}{\lambda_2} \frac{2}{d_{\min}} \quad (1)$$

155 where $\lambda_2' \geq 0$ is the *spectral gap*, i.e. the first non-zero eigenvalue of $\mathcal{L} = \mathbf{I} - \mathbf{D}^{-1/2} \mathbf{A} \mathbf{D}^{-1/2}$
 156 (normalized Laplacian [37], where \mathbf{D} is the degree matrix and \mathbf{A} , the adjacency matrix); $\text{vol}(G)$ is
 157 the volume of the graph (sum of degrees); d_u and d_v are the degrees of nodes u and v , respectively;
 158 and d_{\min} is the minimum degree of the graph.

159 The term $CT_{uv}/\text{vol}(G)$ in Eq. 1 is referred to as the *effective resistance*, R_{uv} , between nodes u and
 160 v . The bound states that the effective resistance between two nodes in the graph converges to or
 161 diverges from $(1/d_u + 1/d_v)$, depending on whether the graph’s spectral gap diverges from or tends
 162 to zero. The larger the spectral gap, the closer $CT_{uv}/\text{vol}(G)$ will be to $\frac{1}{d_u} + \frac{1}{d_v}$ and hence the less
 163 informative the commute times will be.

164 We propose two novel MPNNs layers based on each side of the inequality in Eq. 1: CT-LAYER,
 165 focuses on the left-hand side, and GAP-LAYER, on the right-hand side. The use of each layer
 166 depends on the nature of the network and the task at hand. In a graph classification task (our focus),
 167 CT-LAYER is expected to yield good results when the graph’s spectral gap is small; conversely,
 168 GAP-LAYER would be the layer of choice in graphs with large spectral gap.

169 The Lovász bound was later refined by von Luxburg et al. [38]. App. A.2.2 presents this bound along
 170 with its relationship with R_{uv} as a global measure of node similarity. Once we have defined both
 171 sides of the Lovász bound, we proceed to describe their implications for graph rewiring.

172 3.2 CT-LAYER: Commute Times for Graph Rewiring

173 We focus first on the left-hand side of the Lovász bound which concerns the effective resistances
 174 $CT_{uv}/\text{vol}(G) = R_{uv}$ (or commute times)¹ between any two nodes in the graph.

175 **Spectral Sparsification leads to Commute Times.** Graph sparsification in undirected graphs
 176 may be formulated as finding a graph $H = (V, E')$ that is *spectrally similar* to the original graph
 177 $G = (V, E)$ with $E' \subset E$. Thus, the spectra of their Laplacians, \mathbf{L}_G and \mathbf{L}_H should be similar.

178 **Theorem 1** (Spielman and Srivastava [39]). *Let $\text{Sparsify}(G, q) \rightarrow G'$ be a sampling algorithm of*
 179 *graph $G = (V, E)$, where edges $e \in E$ are sampled with probability $q \propto R_e$ (proportional to the*
 180 *effective resistance). For $n = |V|$ sufficiently large and $1/\sqrt{n} < \epsilon \leq 1$, $O(n \log n / \epsilon^2)$ samples are*
 181 *needed to satisfy $\forall \mathbf{x} \in \mathbb{R}^n : (1 - \epsilon) \mathbf{x}^T \mathbf{L}_G \mathbf{x} \leq \mathbf{x}^T \mathbf{L}_{G'} \mathbf{x} \leq (1 + \epsilon) \mathbf{x}^T \mathbf{L}_G \mathbf{x}$, with probability $\geq 1/2$.*

¹We use commute times and effective resistances interchangeably as per their use in the literature

182 The above theorem has a simple explanation in terms of Dirichlet energies. The Laplacian $\mathbf{L} =$
 183 $\mathbf{D} - \mathbf{A} \succcurlyeq 0$, i.e. it is positive semi-definite (all its eigenvalues are non-negative). Then, if we consider
 184 $\mathbf{x} : V \rightarrow \mathbb{R}$ as a real-valued function of the n nodes of $G = (V, E)$, we have that $\mathcal{E}(\mathbf{x}) := \mathbf{x}^T \mathbf{L}_G \mathbf{x} =$
 185 $\sum_{e=(u,v) \in E} (\mathbf{x}_u - \mathbf{x}_v)^2 \geq 0$ for any \mathbf{x} . In particular, the eigenvectors $\mathbf{f} := \{\mathbf{f}_i : \mathbf{L}\mathbf{f}_i = \lambda_i \mathbf{f}_i\}$ are
 186 the set of special functions (mutually orthogonal and normalized) that minimize the energies $\mathcal{E}(\mathbf{f}_i)$,
 187 i.e. they are the orthogonal functions with the minimal variabilities achievable by the topology of G .
 188 Therefore, Theorem 1 states that any minimal variability of G' is bounded by $(1 \pm \epsilon)$ times that of G
 189 if we sample enough edges with probability $q \propto R_e$.

190 Therefore, the effective resistance is a principled relevance function, since the resulting graph G'
 191 retains the main properties of G . In particular, we have that the spectra of \mathbf{L}_G and $\mathbf{L}_{G'}$ are related by
 192 $(1 - \epsilon)\lambda_i^G \leq \lambda_i^{G'} \leq (1 + \epsilon)\lambda_i^G$: in short $(1 - \epsilon)\mathbf{L}_G \preceq \mathbf{L}_{G'} \preceq (1 + \epsilon)\mathbf{L}_G$. This is a direct result of
 193 the theorem since $\lambda_i = \frac{\mathcal{E}(\mathbf{f}_i)}{\mathbf{f}_i^T \mathbf{f}_i}$ are the normalized minimal variabilities.

194 This first result implies that edge sampling based on effective resistances (or commute times) is a
 195 principled way to rewire a graph while preserving its original structure. Next, we present what is a
 196 commute times embedding and how it can be spectrally computed.

197 **Commute Times Embedding.** The choice of effective resistances in Theorem 1 is explained by
 198 the fact that R_{uv} can be computed from $R_{uv} = (\mathbf{e}_u - \mathbf{e}_v)^T \mathbf{L}^+ (\mathbf{e}_u - \mathbf{e}_v)$, where \mathbf{e}_u is the unit vector
 199 with a unit value at u and zero elsewhere. $\mathbf{L}^+ = \sum_{i \geq 2} \lambda_i^{-1} \mathbf{f}_i \mathbf{f}_i^T$, where \mathbf{f}_i, λ_i are the eigenvectors
 200 and eigenvalues of \mathbf{L} , is the pseudo-inverse or Green's function of $G = (V, E)$ if it is connected, and
 201 from the theorem we also have $(1 + \epsilon)^{-1} \mathbf{L}_G^+ \preceq \mathbf{L}_{G'}^+ \preceq (1 - \epsilon)^{-1} \mathbf{L}_G^+$.

202 The Green's function leads to envision R_{uv} (and therefore CT_{uv}) as *metrics* relating pairs of nodes of
 203 G . For instance $\mathbf{R}_{uv} = \mathbf{L}_{uu}^+ + \mathbf{L}_{vv}^+ - 2\mathbf{L}_{uv}^+$, is the resistance distance [40] i.e., as noted by Qiu and
 204 Hancock [41] the elements \mathbf{L}_{uv}^+ encode dot products between the *embeddings* \mathbf{z}_u and \mathbf{z}_v of u and v .
 205 As a result, the latent space can not only be described spectrally but also in a *parameter free*-manner,
 206 which is not the case for other spectral embeddings, such as heat kernel or diffusion maps as they rely
 207 on a time parameter t . More precisely, the embedding matrix \mathbf{Z} whose columns contain the nodes'
 208 embeddings is given by:

$$\mathbf{Z} := \sqrt{\text{vol}(G)} \Lambda^{-1/2} \mathbf{F}^T = \sqrt{\text{vol}(G)} \Lambda'^{-1/2} \mathbf{G}^T \mathbf{D}^{-1/2} \quad (2)$$

209 where Λ is the diagonal matrix of the unnormalized Laplacian \mathbf{L} eigenvalues and \mathbf{F} is the matrix of
 210 their associated eigenvectors. Similarly, Λ' contains the eigenvalues of the normalized Laplacian \mathcal{L}
 211 and \mathbf{G} the eigenvectors. We have $\mathbf{F} = \mathbf{G} \mathbf{D}^{-1/2}$ or $\mathbf{f}_i = \mathbf{g}_i \mathbf{D}^{-1/2}$, where \mathbf{D} is the degree matrix.

212 Finally, the commute times are given by the Euclidean distances between the embeddings $CT_{uv} =$
 213 $\|\mathbf{z}_u - \mathbf{z}_v\|^2$. Their spectral form is

$$R_{uv} = \frac{CT_{uv}}{\text{vol}(G)} = \sum_{i=2}^n \frac{1}{\lambda_i} (\mathbf{f}_i(u) - \mathbf{f}_i(v))^2 = \sum_{i=2}^n \frac{1}{\lambda_i} \left(\frac{\mathbf{g}_i(u)}{\sqrt{d_u}} - \frac{\mathbf{g}_i(v)}{\sqrt{d_v}} \right)^2 \quad (3)$$

214 Note how in Eq. 3 the commute times rely on the *Fiedler vector* \mathbf{f}_2 (or \mathbf{g}_2) downscaled by the *spectral*
 215 *gap* λ_2 (or more formally λ_2'). The downscaled Fiedler vector dominates the expansion because the
 216 Fiedler vector is the solution to the relaxed ratio-cut problem. This is consistent with the fact that
 217 p -resistances become the inverse of mincut when $p \rightarrow \infty$.

218 **Commute Times as an Optimization Problem.** In this section, we demonstrate how the CTs may
 219 be computed as an optimization problem by means of a differentiable layer in a GNN. Constraining
 220 neighboring nodes to have a similar embedding leads to

$$\mathbf{Z} = \arg \min_{\mathbf{Z}^T \mathbf{Z} = \mathbf{I}} \frac{\sum_{u,v} \|\mathbf{z}_u - \mathbf{z}_v\|^2 \mathbf{A}_{uv}}{\sum_{u,v} \mathbf{Z}_{uv}^2 d_u} = \frac{\sum_{(u,v) \in E} \|\mathbf{z}_u - \mathbf{z}_v\|^2}{\sum_{u,v} \mathbf{Z}_{uv}^2 d_u} = \frac{\text{Tr}[\mathbf{Z}^T \mathbf{L} \mathbf{Z}]}{\text{Tr}[\mathbf{Z}^T \mathbf{D} \mathbf{Z}]}, \quad (4)$$

221 which reveals that CTs embeddings result from a Laplacian regularization down-weighted by the
 222 degree. As a result, *frontier* nodes or hubs –i.e. nodes with inter-community edges– which tend to
 223 have larger degrees than those lying inside their respective communities will be embedded far away
 224 from their neighbors, increasing the *distance* between communities. Note that the above *quotient of*
 225 *traces* formulation is easily differentiable and different from $\text{Tr}[\frac{\mathbf{Z}^T \mathbf{L} \mathbf{Z}}{\mathbf{Z}^T \mathbf{D} \mathbf{Z}}]$ proposed in [41].

226 With the above elements we define CT-LAYER, the first rewiring layer proposed in this paper. See
 227 Figure 2 for a graphical representation of the layer.

228

229 **Definition 1 (CT-Layer).** Given the matrix $\mathbf{X}_{n \times F}$ encoding the features of the nodes after any
 230 message passing (MP) layer, $\mathbf{Z}_{n \times O(n)} = \tanh(\text{MLP}(\mathbf{X}))$ learns the association $\mathbf{X} \rightarrow \mathbf{Z}$ while \mathbf{Z} is
 231 optimized according to the loss $L_{CT} = \frac{\text{Tr}[\mathbf{Z}^T \mathbf{L} \mathbf{Z}]}{\text{Tr}[\mathbf{Z}^T \mathbf{D} \mathbf{Z}]} + \left\| \frac{\mathbf{Z}^T \mathbf{Z}}{\|\mathbf{Z}^T \mathbf{Z}\|_F} - \mathbf{I}_n \right\|_F$. This results in the following
 232 resistance diffusion $\mathbf{T}^{CT} = \mathbf{R}(\mathbf{Z}) \odot \mathbf{A}$, i.e. the Hadamard product between the resistance distance
 233 and the adjacency matrix, providing as input to the subsequent MP layer a learnt convolution matrix.
 234 We set $\mathbf{R}(\mathbf{Z})$ to the pairwise Euclidean distances of the node embeddings in \mathbf{Z} divided by $\text{vol}(G)$.

235 Thus, CT-LAYER learns the CTs and rewires an input graph according to them: the edges with
 236 maximal resistance will tend to be the most important edges so as to preserve the topology of the
 237 graph.

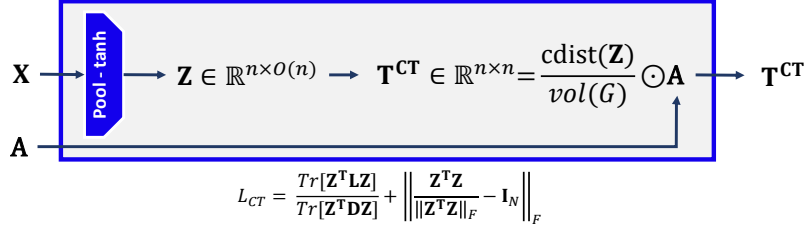


Figure 2: Detailed depiction of CT-LAYER, where `cdist` refers to the matrix of pairwise Euclidean distances between the node embeddings in \mathbf{Z} .

238 Below, we present the relationship between the CTs and the graph’s bottleneck and curvature.

239 **\mathbf{T}^{CT} and Graph Bottlenecks.** Beyond the principled sparsification of \mathbf{T}^{CT} (enabled by Theo-
 240 rem 1), this layer rewires the graph $G = (E, V)$ in such a way that edges with maximal resistance
 241 will tend to be the most critical to preserve the topology of the graph. More precisely, although
 242 $\sum_{e \in E} R_e = n - 1$, the bulk of the resistance distribution will be located at graph bottlenecks, if they
 243 exist. Otherwise, their magnitude is upper-bounded and the distribution becomes more uniform.

244 Graph bottlenecks are controlled by the graph’s conductance or Cheeger constant, $h_G = \min_{S \subseteq V} h_S$,
 245 where: $h_S = \frac{|\partial S|}{\min(\text{vol}(S), \text{vol}(\bar{S}))}$, $\partial S = \{e = (u, v) : u \in S, v \in \bar{S}\}$ and $\text{vol}(S) = \sum_{u \in S} d_u$.

246 The interplay between the graph’s conductance and effective resistances is given by:

247 **Theorem 2** (Alev et al. [42]). Given a graph $G = (V, E)$, a subset $S \subseteq V$ with $\text{vol}(S) \leq \text{vol}(G)/2$,

248

$$h_S \geq \frac{c}{\text{vol}(S)^{1/2-\epsilon}} \iff |\partial S| \geq c \cdot \text{vol}(S)^{1/2-\epsilon}, \quad (5)$$

249 for some constant c and $\epsilon \in [0, 1/2]$. Then, $R_{uv} \leq \left(\frac{1}{d_u^{2\epsilon}} + \frac{1}{d_v^{2\epsilon}} \right) \cdot \frac{1}{c \cdot c^{2\epsilon}}$ for any pair u, v .

250 According to this theorem, the larger the graph’s bottleneck, the tighter the bound on R_{uv} are.
 251 Moreover, $\max(R_{uv}) \leq 1/h_S^2$, i.e., the resistance is bounded by the square of the bottleneck.

252 This bound partially explains the rewiring of the graph in Figure 1-center. As seen in the Figure,
 253 rewiring using CT-LAYER sparsifies the graph and assigns larger weights to the edges located in
 254 the graph’s bottleneck. The interplay between the above theorem and Theorem 1 is described in
 255 App. A.1.

256 Recent work has proposed using curvature for graph rewiring. We outline below the relationship
 257 between CTs and curvature.

258 **Effective Resistances and Curvature.** Topping et al. [20] propose an approach for graph rewiring,
 259 where the relevance function is given by the Ricci curvature. However, this measure is non-
 260 differentiable. More recent definitions of curvature [24] have been formulated based on resistance
 261 distances that would be differentiable using our approach. The resistance curvature of an edge
 262 $e = (u, v)$ is $\kappa_{uv} := 2(p_u + p_v)/R_{uv}$ where $p_u := 1 - \frac{1}{2} \sum_{u \sim w} R_{uw}$ is the node’s curvature.

263 Relevant properties of the edge resistance curvature are discussed in App. A.1.3, along with a related
 264 Theorem proposed in Devriendt and Lambiotte [24].

265 3.3 GAP-LAYER: Spectral Gap Optimization for Graph Rewiring

266 The right-hand side of the Lovász bound in Eq. 1 relies on the graph’s spectral gap λ'_2 , such that the
 267 larger the spectral gap, the closer the commute times would be to their non-informative regime. Note
 268 that the spectral gap is typically large in commonly observed graphs –such as communities in social
 269 networks which may be bridged by many edges [43]– and, hence, in these cases it would be desirable
 270 to rewire the adjacency matrix \mathbf{A} so that λ'_2 is minimized.

271 In this section, we explain how to rewire the graph’s adjacency matrix \mathbf{A} to minimize the spectral gap.
 272 We propose using the gradient of λ_2 wrt each component of $\tilde{\mathbf{A}}$. Then, we can compute these gradient
 273 either using Laplacians ($\tilde{\mathbf{L}}$, with Fiedler λ_2) or normalized Laplacians ($\tilde{\mathcal{L}}$, with Fiedler λ'_2). We also
 274 present an approximation of the Fiedler vectors needed to compute those gradients, and propose
 275 computing them as a GNN Layer called the GAP-LAYER. A detailed schematic of GAP-LAYER is
 276 shown in Figure 3.

277 **Ratio-cut (Rcut) Approximation.** We propose to rewire the adjacency matrix, \mathbf{A} , so that λ_2 is
 278 minimized. We consider a matrix $\tilde{\mathbf{A}}$ close to \mathbf{A} that satisfies $\tilde{\mathbf{L}}\mathbf{f}_2 = \lambda_2\mathbf{f}_2$, where \mathbf{f}_2 is the solution to
 279 the ratio-cut relaxation [44]. Following [45], the gradient of λ_2 wrt each component of $\tilde{\mathbf{A}}$ is given by

$$\nabla_{\tilde{\mathbf{A}}}\lambda_2 := \text{Tr} \left[(\nabla_{\tilde{\mathbf{L}}}\lambda_2)^T \cdot \nabla_{\tilde{\mathbf{A}}}\tilde{\mathbf{L}} \right] = \text{diag}(\mathbf{f}_2\mathbf{f}_2^T)\mathbf{1}\mathbf{1}^T - \mathbf{f}_2\mathbf{f}_2^T \quad (6)$$

280 where $\mathbf{1}$ is the vector of n ones; and $[\nabla_{\tilde{\mathbf{A}}}\lambda_2]_{ij}$ is the gradient of λ_2 wrt $\tilde{\mathbf{A}}_{uv}$. The driving force of
 281 this gradient relies on the correlation $\mathbf{f}_2\mathbf{f}_2^T$. Using this gradient to minimize λ_2 results in breaking
 282 the graph’s bottleneck while preserving simultaneously the inter-cluster structure. We delve into this
 283 matter in App. A.2.

284 **Normalized-cut (Ncut) Approximation.** Similarly, considering now λ'_2 for rewiring leads to

$$\begin{aligned} \nabla_{\tilde{\mathbf{A}}}\lambda'_2 &:= \text{Tr} \left[(\nabla_{\tilde{\mathcal{L}}}\lambda'_2)^T \cdot \nabla_{\tilde{\mathbf{A}}}\tilde{\mathcal{L}} \right] = \\ &\mathbf{d}' \left\{ \mathbf{g}_2^T \tilde{\mathbf{A}}^T \tilde{\mathbf{D}}^{-1/2} \mathbf{g}_2 \right\} \mathbf{1}^T + \mathbf{d}' \left\{ \mathbf{g}_2^T \tilde{\mathbf{A}} \tilde{\mathbf{D}}^{-1/2} \mathbf{g}_2 \right\} \mathbf{1}^T + \tilde{\mathbf{D}}^{-1/2} \mathbf{g}_2 \mathbf{g}_2^T \tilde{\mathbf{D}}^{-1/2} \end{aligned} \quad (7)$$

285 where \mathbf{d}' is a $n \times 1$ vector including derivatives of degree wrt adjacency and related terms. This
 286 gradient relies on the Fiedler vector \mathbf{g}_2 (the solution to the normalized-cut relaxation), and on the
 287 incoming and outgoing one-hop random walks. This approximation breaks the bottleneck while
 288 preserving the global topology of the graph (Figure 1-left). More details and proof are included in
 289 App. A.2.

290 We present next an approximation of the Fiedler vector, followed by a proposed new layer in the
 291 GNN called the GAP-LAYER to learn how to minimize the spectral gap of the graph.

292 **Approximating the Fiedler vector.** Given that $\mathbf{g}_2 = \tilde{\mathbf{D}}^{1/2}\mathbf{f}_2$, we can obtain the normalized-cut
 293 gradient in terms of \mathbf{f}_2 . From [17] we have that

$$\mathbf{f}_2(u) = \begin{cases} +1/\sqrt{n} & \text{if } u \text{ belongs to the first cluster} \\ -1/\sqrt{n} & \text{if } u \text{ belongs to the second cluster} \end{cases} + O\left(\frac{\log n}{n}\right) \quad (8)$$

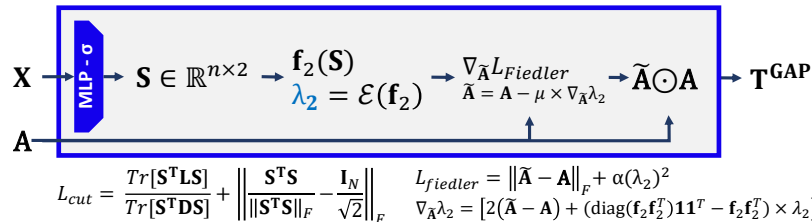


Figure 3: GAP-LAYER (Rcut). For GAP-LAYER (Ncut), substitute $\nabla_{\tilde{\mathbf{A}}}\lambda_2$ by Eq. 7

294 **Definition 2** (GAP-Layer). Given the matrix $\mathbf{X}_{n \times F}$ encoding the features of the nodes after any
 295 message passing (MP) layer, $\mathbf{S}_{n \times 2} = \text{Softmax}(\text{MLP}(\mathbf{X}))$ learns the association $\mathbf{X} \rightarrow \mathbf{S}$ while \mathbf{S} is
 296 optimized according to the loss $L_{\text{Cut}} = -\frac{\text{Tr}[\mathbf{S}^T \mathbf{A} \mathbf{S}]}{\text{Tr}[\mathbf{S}^T \mathbf{D} \mathbf{S}]} + \left\| \frac{\mathbf{S}^T \mathbf{S}}{\|\mathbf{S}^T \mathbf{S}\|_F} - \frac{\mathbf{I}_n}{\sqrt{2}} \right\|_F$. Then the Fiedler vector
 297 \mathbf{f}_2 is approximated by applying a softmaxed version of Eq. 8 and considering the loss $L_{\text{Fiedler}} =$
 298 $\|\tilde{\mathbf{A}} - \mathbf{A}\|_F + \alpha(\lambda_2^*)^2$, where $\lambda_2^* = \lambda_2$ if we use the ratio-cut approximation (and gradient) and
 299 $\lambda_2^* = \lambda_2'$ if we use the normalized-cut approximation and gradient. This returns $\tilde{\mathbf{A}}$ and the GAP
 300 diffusion $\mathbf{T}^{\text{GAP}} = \tilde{\mathbf{A}}(\mathbf{S}) \odot \mathbf{A}$ results from minimizing $L_{\text{GAP}} := L_{\text{Cut}} + L_{\text{Fiedler}}$.

301 4 Experiments and Discussion

302 In this section, we study the properties and performance of CT-LAYER and GAP-LAYER in a graph
 303 classification task with several benchmark datasets. To illustrate the merits of our approach, we
 304 compare CT-LAYER and GAP-LAYER with 3 state-of-the-art diffusion and curvature-based graph
 305 rewiring methods. Note that the aim of the evaluation is to shed light on the properties of both layers
 306 and illustrate their inductive performance, not to perform a benchmark comparison with all previously
 307 proposed graph rewiring methods.

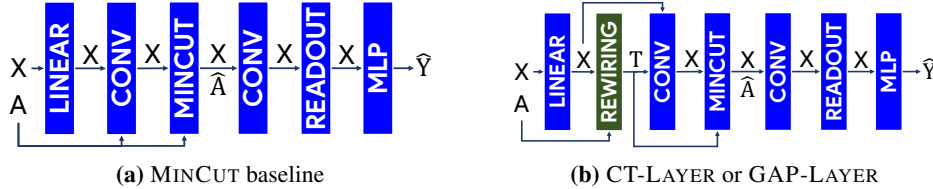


Figure 4: GNN models used in the experiments. Left: MinCut Baseline model. Right: CT-LAYER or GAP-LAYER models, depending on what method is used for rewiring.

308 **Baselines:** The first baseline architecture is based on **MINCUT Pool** [33] and it is shown in Figure 4a.
 309 It is the base GNN that we use for graph classification without rewiring. MINCUT Pool layer learns
 310 $(\mathbf{A}_{n \times n}, \mathbf{X}_{n \times F}) \rightarrow (\mathbf{A}'_{k \times k}, \mathbf{X}_{k \times F})$, being $k < n$ the new number of node clusters. **The first baseline**
 311 **strategy using graph rewiring is k -NN graphs [46], where weights of the edges are computed based**
 312 **on feature similarity.** The next two baselines are graph rewiring methods that belong to the same
 313 family of methods as DIFFWIRE, i.e. methods based on diffusion and curvature, namely **DIGL**
 314 (PPR) [25] and **SDRF** [20]. DIGL is a diffusion-based preprocessing method within the family of
 315 metric-based GSL approaches. We set the teleporting probability $\alpha = 0.001$ and ϵ is set to keep the
 316 same average degree for each graph. Once preprocessed with DIGL, the graphs are provided as input
 317 to the MinCut Pool (Baseline1) architecture. The third baseline model is SDRF, which performs
 318 curvature-based rewiring. SDRF is also a preprocessing method which has 3 parameters that are
 319 highly graph-dependent. We set these parameters to $\tau = 20$ and $C^+ = 0$ for all experiments as per
 320 [20]. The number of iterations is estimated dynamically according to $0.7 * |V|$ for each graph.

321 Both DIGL and SDRF aim to preserve the global topology of the graph but require optimizing their
 322 parameters for each input graph via hyper-parameter search. In a graph classification task, this search
 323 is $O(n^3)$ per graph. Details about the parameter tuning in these methods can be found in App. A.3.3.

324 To shed light on the performance and properties of CT-LAYER and GAP-LAYER, we add the
 325 corresponding layer in between Linear(\mathbf{X}) $\xrightarrow{*}$ Conv1(\mathbf{A}, \mathbf{X}). We build 3 different models: CT-
 326 LAYER, GAP-LAYER (Rcut), GAP-LAYER (Ncut), depending on the layer used. For CT-LAYER,
 327 we learn \mathbf{T}^{CT} which is used as a convolution matrix afterwards. For GAP-LAYER, we learn \mathbf{T}^{GAP}
 328 either using the Rcut or the Ncut approximations. A schematic of the architectures is shown in
 329 Figure 4b and in App. A.3.2.

330 As shown in Table 1, we use in our experiments common benchmark datasets for graph classification.
 331 We select datasets both with features and featureless, in which case we use the degree as the node
 332 features. These datasets are diverse regarding the topology of their networks: REDDIT-B, IMDB-B
 333 and COLLAB contain truncate scale-free graphs (social networks), whereas MUTAG and PROTEINS
 334 contain graphs from biology or chemistry. In addition, we use two synthetic datasets with 2 classes:
 335 Erdős-Rényi with $p_1 \in [0.3, 0.5]$ and $p_2 \in [0.4, 0.8]$ and Stochastic block model (SBM) with
 336 parameters $p_1 = 0.8, p_2 = 0.5, q_1 \in [0.1, 0.15]$ and $q_2 \in [0.01, 0.1]$. More details in App. A.3.1.

Table 1: Experimental results on common graph classification benchmarks. **Red** denotes the best model row-wise and **Blue** marks the runner-up. ***** means degree as node feature.

	MinCutPool	k -NN	DIGL	SDRF	CT-LAYER	GAP-LAYER (R)	GAP-LAYER (N)
REDDIT-B*	66.53±4.4	64.40±3.8	76.02±4.3	65.3±7.7	78.45±4.5	77.63±4.9	76.00±5.3
IMDB-B*	60.75±7.0	55.20±4.3	59.35±7.7	59.2±6.9	69.84±4.6	69.93±3.3	68.80±3.1
COLLAB*	58.00±6.2	58.33±11	57.51±5.9	56.60±10	69.87±2.4	64.47±4.0	65.89±4.9
MUTAG	84.21±6.3	87.58±4.1	85.00±5.6	82.4±6.8	87.58±4.4	86.90±4.0	86.90±4.0
PROTEINS	74.84±2.3	76.76±2.5	74.49±2.8	74.4±2.7	75.38±2.9	75.03±3.0	75.34±2.1
SBM*	53.00±9.9	50.00±0.0	56.93±12	54.1±7.1	81.40±11	90.80±7.0	92.26±2.9
Erdős-Rényi*	81.86±6.2	63.40±3.9	81.93±6.3	73.6±9.1	79.06±9.8	79.26±10	82.26±3.2

337 Table 1 reports average accuracies and standard deviation on 10 random data splits, using 85/15
 338 stratified train-test split, training during 60 epochs and reporting the results of the last epoch for each
 339 random run. We use Pytorch Geometric framework and our code is publicly available².

340 The experiments support our hypothesis that rewiring based on CT-LAYER and GAP-LAYER
 341 improves the performance of the baselines on graph classification. Since both layers are differentiable,
 342 they learn how to rewire unseen graphs. The improvements are significant in graphs where social
 343 components arise (REDDITB, IMDBB, COLLAB), i.e. graphs with small world properties and
 344 power-law degree distributions with a topology based on hubs and authorities. These are graphs
 345 where bottlenecks arise easily and our approach is able to properly rewire the graphs. However, the
 346 improvements observed in planar or grid networks (MUTAG and PROTEINS) are more limited: the
 347 bottleneck does not seem to be critical for the graph classification task.

348 Moreover, CT-LAYER and GAP-LAYER perform better in graphs with featureless nodes than graphs
 349 with node features because it is able to leverage the information encoded in the topology of the
 350 graphs. Note that in attribute-based graphs, the weights of the attributes typically overwrite the
 351 graph’s structure in the classification task, whereas in graphs without node features, the information
 352 is encoded in the graph’s structure. **Thus, k -NN rewiring outperforms every other rewiring method in
 353 graph classification where graphs has node features.** App. A.3.4 contains an in-depth analysis of the
 354 graphs latent space of the readout layer produced by each model. **In addition, the compare the node
 355 CT embeddings, Z , predicted by CT-LAYER with the spectral embeddings given by equation 2.**

356 **In addition, as an ablation study, we performed preliminary experiments in node classification to
 357 show the promising potential of CT-LAYER in this task, both for improving diffusion in heterophilic
 358 graphs, and for using the learned CTE from CT-LAYER (Z) as a novel method for learning node
 359 positional encodings (PE) [35, 36]. These results are further discussed in Appendix A.3.5.**

360 **CT-LAYER vs GAP-LAYER.** The real-world datasets explored in this paper are characterized by
 361 mild bottlenecks from the perspective of the Lovász bound. For completion, we have included two
 362 synthetic datasets (SBM and Erdős-Rényi) where the Lovász bound is very restrictive. As a result,
 363 CT-LAYER is outperformed by GAP-LAYER in SBM. Note that the results on the synthetic datasets
 364 suffer from large variability. **As a general rule of thumb, the smaller the graph’s bottleneck (defined
 365 as the ratio between the number of inter-community edges and the number of intra-community edges),
 366 the more useful the CT-LAYER is because the rewired graph will be sparsified in the communities
 367 but will preserve the edges in the gap.** Conversely, the larger the bottleneck, the more useful the
 368 GAP-Layer is.

369 5 Conclusion and Future Work

370 In this paper, we have proposed DIFFWIRE, a unified framework for graph rewiring that links the
 371 two components of the Lovász bound: CTs and the spectral gap. We have presented two novel, fully
 372 differentiable and inductive rewiring layers: CT-LAYER and GAP-LAYER. We have empirically
 373 evaluated these layers on benchmark datasets for graph classification with competitive results when
 374 compared to SoTA baselines, specially in graphs where the the nodes have no attributes and have
 375 small-world properties.

376 In future work, we plan to test our approach in other graph-related tasks and intend to apply DIFFWIRE
 377 to real-world applications, particularly in social networks, which have unique topology, statistics and
 378 direct implications in society.

²<https://anonymous.4open.science/r/DiffWireLoG22/readme.md>

References

- 379
- 380 [1] Marco Gori, Gabriele Monfardini, and Franco Scarselli. A new model for learning in graph domains. In
381 *Proceedings. 2005 IEEE international joint conference on neural networks*, volume 2, pages 729–734,
382 2005. URL <https://ieeexplore.ieee.org/document/1555942>. 1
- 383 [2] Franco Scarselli, Marco Gori, Ah Chung Tsoi, Markus Hagenbuchner, and Gabriele Monfardini. The
384 graph neural network model. *IEEE transactions on neural networks*, 20(1):61–80, 2008. URL <https://ieeexplore.ieee.org/document/4700287>. 1
- 385
- 386 [3] Thomas N. Kipf and Max Welling. Semi-supervised classification with graph convolutional networks. In
387 *International Conference on Learning Representations (ICLR)*, 2017. URL <https://openreview.net/forum?id=SJU4ayYgl>. 1
- 388
- 389 [4] Justin Gilmer, Samuel S. Schoenholz, Patrick F. Riley, Oriol Vinyals, and George E. Dahl. Neural message
390 passing for quantum chemistry. In *Proceedings of the 34th International Conference on Machine Learning*,
391 ICML, page 1263–1272, 2017. 1
- 392 [5] Thomas N Kipf and Max Welling. Variational graph auto-encoders. In *NeurIPS Workshop on Bayesian*
393 *Deep Learning*, 2016. URL http://bayesiandeeplearning.org/2016/papers/BDL_16.pdf. 1
- 394 [6] Shaosheng Cao, Wei Lu, and Qionгкаi Xu. Deep neural networks for learning graph representations. In
395 *Proceedings of the AAAI Conference on Artificial Intelligence*, volume 30, 2016. URL <https://ojs.aaai.org/index.php/AAAI/article/view/10179>. 1
- 396
- 397 [7] Fei Tian, Bin Gao, Qing Cui, Enhong Chen, and Tie-Yan Liu. Learning deep representations for graph
398 clustering. In *Proceedings of the AAAI Conference on Artificial Intelligence*, 2014. URL <https://ojs.aaai.org/index.php/AAAI/article/view/8916>. 1
- 399
- 400 [8] Zonghan Wu, Shirui Pan, Fengwen Chen, Guodong Long, Chengqi Zhang, and Philip S. Yu. A compre-
401 hensive survey on graph neural networks. *IEEE Transactions on Neural Networks and Learning Systems*, 32
402 (1):4–24, 2021. URL <https://ieeexplore.ieee.org/document/9046288>. 1, 2
- 403 [9] Petar Veličković, Guillem Cucurull, Arantxa Casanova, Adriana Romero, Pietro Liò, and Yoshua Bengio.
404 Graph Attention Networks. *International Conference on Learning Representations*, 2018. URL <https://openreview.net/forum?id=rJXMpikCZ>. 1
- 405
- 406 [10] Shaked Brody, Uri Alon, and Eran Yahav. How attentive are graph attention networks? In *International*
407 *Conference on Learning Representations*, 2022. URL <https://openreview.net/forum?id=F72ximsx7C1>. 1
- 408 [11] Keyulu Xu, Weihua Hu, Jure Leskovec, and Stefanie Jegelka. How powerful are graph neural networks?
409 In *International Conference on Learning Representations*, 2019. URL <https://openreview.net/forum?id=ryGs6iA5Km>. 1
- 410
- 411 [12] Will Hamilton, Zhitaoying, and Jure Leskovec. Inductive representation learning on large graphs. In
412 *Advances in Neural Information Processing Systems*, 2017. URL <https://proceedings.neurips.cc/paper/2017/file/5dd9db5e033da9c6fb5ba83c7a7e9bea9-Paper.pdf>. 1, 3
- 413
- 414 [13] Qimai Li, Zhichao Han, and Xiao-Ming Wu. Deeper insights into graph convolutional networks for
415 semi-supervised learning. In *Proceedings of the Thirty-Second AAAI Conference on Artificial Intelligence*,
416 2018. URL <https://ojs.aaai.org/index.php/AAAI/article/view/11604>. 1
- 417 [14] Uri Alon and Eran Yahav. On the bottleneck of graph neural networks and its practical implications.
418 In *International Conference on Learning Representations*, 2021. URL <https://openreview.net/forum?id=i800Ph0CVH2>. 1, 2
- 419
- 420 [15] László Lovász. Random walks on graphs. *Combinatorics, Paul erdos is eighty*, 2(1-46):4, 1993. URL
421 <https://web.cs.elte.hu/~lovasz/erdos.pdf>. 1, 2, 4
- 422 [16] Pablo Barceló, Egor V. Kostylev, Mikael Monet, Jorge Pérez, Juan Reutter, and Juan Pablo Silva. The
423 logical expressiveness of graph neural networks. In *International Conference on Learning Representations*,
424 2020. URL <https://openreview.net/forum?id=r11z7AEKvB>. 1
- 425 [17] NT Hoang, Takanori Maehara, and Tsuyoshi Murata. Revisiting graph neural networks: Graph filtering
426 perspective. In *25th International Conference on Pattern Recognition (ICPR)*, pages 8376–8383, 2021.
427 URL <https://ieeexplore.ieee.org/document/9412278>. 2, 7, 18
- 428 [18] Kenta Oono and Taiji Suzuki. Graph neural networks exponentially lose expressive power for node
429 classification. In *International Conference on Learning Representations*, 2020. URL <https://openreview.net/forum?id=S11d02EFPr>.
- 430
- 431 [19] Jie Zhou, Ganqu Cui, Zhengyan Zhang, Cheng Yang, Zhiyuan Liu, and Maosong Sun. Graph neural
432 networks: A review of methods and applications. *CoRR*, abs/1812.08434, 2018. URL <http://arxiv.org/abs/1812.08434>. 2
- 433

- 434 [20] Jake Topping, Francesco Di Giovanni, Benjamin Paul Chamberlain, Xiaowen Dong, and Michael M.
435 Bronstein. Understanding over-squashing and bottlenecks on graphs via curvature. In *International*
436 *Conference on Learning Representations*, 2022. URL <https://openreview.net/forum?id=7UmjRGZp-A>. 2, 3, 6,
437 8, 17, 22
- 438 [21] Petar Veličković. Message passing all the way up. In *ICLR 2022 Workshop on Geometrical and Topological*
439 *Representation Learning*, 2022. URL <https://openreview.net/forum?id=Bc8GiEZkTe5>. 2
- 440 [22] Yu Rong, Wenbing Huang, Tingyang Xu, and Junzhou Huang. Dropedge: Towards deep graph convolutional
441 networks on node classification. In *International Conference on Learning Representations*, 2020.
442 URL <https://openreview.net/forum?id=Hkx1qkrKPr>. 2, 3
- 443 [23] Anees Kazi, Luca Cosmo, Seyed-Ahmad Ahmadi, Nassir Navab, and Michael Bronstein. Differentiable
444 graph module (dgm) for graph convolutional networks. *IEEE Transactions on Pattern Analysis and*
445 *Machine Intelligence*, pages 1–1, 2022. URL <https://ieeexplore.ieee.org/document/9763421>. 2, 3
- 446 [24] Karel Devriendt and Renaud Lambiotte. Discrete curvature on graphs from the effective resistance. *arXiv*
447 *preprint arXiv:2201.06385*, 2022. doi: 10.48550/ARXIV.2201.06385. URL [https://arxiv.org/abs/2201.](https://arxiv.org/abs/2201.06385)
448 [06385](https://arxiv.org/abs/2201.06385). 2, 6, 7, 17
- 449 [25] Johannes Klicpera, Stefan Weissenberger, and Stephan Günnemann. Diffusion improves graph learning. In
450 *Advances in Neural Information Processing Systems*, 2019. URL [https://proceedings.neurips.cc/paper/](https://proceedings.neurips.cc/paper/2019/file/23c894276a2c5a16470e6a31f4618d73-Paper.pdf)
451 [2019/file/23c894276a2c5a16470e6a31f4618d73-Paper.pdf](https://proceedings.neurips.cc/paper/2019/file/23c894276a2c5a16470e6a31f4618d73-Paper.pdf). 3, 8, 22
- 452 [26] Peter W Battaglia, Jessica B Hamrick, Victor Bapst, Alvaro Sanchez-Gonzalez, Vinicius Zambaldi,
453 Mateusz Malinowski, Andrea Tacchetti, David Raposo, Adam Santoro, Ryan Faulkner, et al. Relational
454 inductive biases, deep learning, and graph networks. *arXiv preprint arXiv:1806.01261*, 2018. URL
455 <https://arxiv.org/abs/1806.01261>. 3
- 456 [27] Fabrizio Frasca, Emanuele Rossi, Davide Eynard, Benjamin Chamberlain, Michael Bronstein, and Federico
457 Monti. Sign: Scalable inception graph neural networks. In *ICML 2020 Workshop on Graph Representation*
458 *Learning and Beyond*, 2020. URL <https://gr1plus.github.io/papers/77.pdf>. 3
- 459 [28] Pál András Papp, Karolis Martinkus, Lukas Faber, and Roger Wattenhofer. DropGNN: Random dropouts
460 increase the expressiveness of graph neural networks. In *Advances in Neural Information Processing*
461 *Systems*, 2021. URL <https://openreview.net/forum?id=fpQojkIV5q8>. 3
- 462 [29] Deli Chen, Yankai Lin, Wei Li, Peng Li, Jie Zhou, and Xu Sun. Measuring and relieving the over-
463 smoothing problem for graph neural networks from the topological view. *Proceedings of the AAAI*
464 *Conference on Artificial Intelligence*, 34(04):3438–3445, Apr. 2020. doi: 10.1609/aaai.v34i04.5747. URL
465 <https://ojs.aaai.org/index.php/AAAI/article/view/5747>. 3
- 466 [30] Yanqiao Zhu, Weizhi Xu, Jinghao Zhang, Yuanqi Du, Jieyu Zhang, Qiang Liu, Carl Yang, and Shu
467 Wu. A survey on graph structure learning: Progress and opportunities. *arXiv PrePrint*, 2021. URL
468 <https://arxiv.org/abs/2103.03036>. 3
- 469 [31] Diego Mesquita, Amauri Souza, and Samuel Kaski. Rethinking pooling in graph neural networks. In
470 *Advances in Neural Information Processing Systems*, 2020. URL [https://proceedings.neurips.cc/paper/](https://proceedings.neurips.cc/paper/2020/file/1764183ef03fc7324eb58c3842bd9a57-Paper.pdf)
471 [2020/file/1764183ef03fc7324eb58c3842bd9a57-Paper.pdf](https://proceedings.neurips.cc/paper/2020/file/1764183ef03fc7324eb58c3842bd9a57-Paper.pdf). 3
- 472 [32] Zhitao Ying, Jiaxuan You, Christopher Morris, Xiang Ren, Will Hamilton, and Jure Leskovec.
473 Hierarchical graph representation learning with differentiable pooling. In *Advances in Neural*
474 *Information Processing Systems*, 2018. URL [https://proceedings.neurips.cc/paper/2018/file/](https://proceedings.neurips.cc/paper/2018/file/e77dbaf6759253c7c6d0efc5690369c7-Paper.pdf)
475 [e77dbaf6759253c7c6d0efc5690369c7-Paper.pdf](https://proceedings.neurips.cc/paper/2018/file/e77dbaf6759253c7c6d0efc5690369c7-Paper.pdf). 3
- 476 [33] Filippo Maria Bianchi, Daniele Grattarola, and Cesare Alippi. Spectral clustering with graph neural
477 networks for graph pooling. In *Proceedings of the 37th International Conference on Machine Learning*,
478 2020. URL <https://proceedings.mlr.press/v119/bianchi20a.html>. 3, 8
- 479 [34] Ladislav Rampáček, Mikhail Galkin, Vijay Prakash Dwivedi, Anh Tuan Luu, Guy Wolf, and Dominique
480 Beaini. Recipe for a General, Powerful, Scalable Graph Transformer. *arXiv:2205.12454*, 2022. URL
481 <https://arxiv.org/pdf/2205.12454.pdf>. 3, 24
- 482 [35] Ameya Velingker, Ali Kemal Sinop, Ira Ktena, Petar Veličković, and Sreenivas Gollapudi. Affinity-aware
483 graph networks. *arXiv preprint arXiv:2206.11941*, 2022. URL <https://arxiv.org/pdf/2206.11941.pdf>. 3, 9,
484 22, 24, 25
- 485 [36] Vijay Prakash Dwivedi and Xavier Bresson. A generalization of transformer networks to graphs. *AAAI*
486 *Workshop on Deep Learning on Graphs: Methods and Applications*, 2021. URL [https://arxiv.org/pdf/](https://arxiv.org/pdf/2012.09699.pdf)
487 [2012.09699.pdf](https://arxiv.org/pdf/2012.09699.pdf). 3, 9, 22, 24
- 488 [37] F. R. K. Chung. *Spectral Graph Theory*. American Mathematical Society, 1997. URL [https://www.](https://www.bibsonomy.org/bibtex/295ef10b5a69a03d8507240b6cf410f8a/folke)
489 [bibsonomy.org/bibtex/295ef10b5a69a03d8507240b6cf410f8a/folke](https://www.bibsonomy.org/bibtex/295ef10b5a69a03d8507240b6cf410f8a/folke). 4
- 490 [38] Ulrike von Luxburg, Agnes Radl, and Matthias Hein. Hitting and commute times in large random
491 neighborhood graphs. *Journal of Machine Learning Research*, 15(52):1751–1798, 2014. URL [http:](http://jmlr.org/papers/v15/vonluxburg14a.html)
492 [/jmlr.org/papers/v15/vonluxburg14a.html](http://jmlr.org/papers/v15/vonluxburg14a.html). 4, 19

- 493 [39] Daniel A. Spielman and Nikhil Srivastava. Graph sparsification by effective resistances. *SIAM Journal on*
494 *Computing*, 40(6):1913–1926, 2011. doi: 10.1137/080734029. URL <https://doi.org/10.1137/080734029>. 4
- 495 [40] D. J. Klein and M. Randić. Resistance distance. *Journal of Mathematical Chemistry*, 12(1):81–95, 1993.
496 doi: 10.1007/BF01164627. URL <https://doi.org/10.1007/BF01164627>. 5, 23
- 497 [41] Huaijun Qiu and Edwin R. Hancock. Clustering and embedding using commute times. *IEEE Transactions*
498 *on Pattern Analysis and Machine Intelligence*, 29(11):1873–1890, 2007. doi: 10.1109/TPAMI.2007.1103.
499 URL <https://ieeexplore.ieee.org/document/4302755>. 5
- 500 [42] Vedat Levi Alev, Nima Anari, Lap Chi Lau, and Shayan Oveis Gharan. Graph Clustering using Effective
501 Resistance. In *9th Innovations in Theoretical Computer Science Conference (ITCS 2018)*, volume 94, pages
502 1–16, 2018. doi: 10.4230/LIPIcs.ITCS.2018.41. URL <http://drops.dagstuhl.de/opus/volltexte/2018/8369>.
503 6, 16, 23
- 504 [43] Emmanuel Abbe. Community detection and stochastic block models: Recent developments. *Journal of*
505 *Machine Learning Research*, 18(177):1–86, 2018. URL <http://jmlr.org/papers/v18/16-480.html>. 7, 19
- 506 [44] Thomas Bühler and Matthias Hein. Spectral clustering based on the graph p-laplacian. In *Proceedings of the*
507 *26th Annual International Conference on Machine Learning, ICML '09*, page 81–88, New York, NY, USA,
508 2009. Association for Computing Machinery. ISBN 9781605585161. doi: 10.1145/1553374.1553385.
509 URL <https://doi.org/10.1145/1553374.1553385>. 7, 19
- 510 [45] Jian Kang and Hanghang Tong. N2n: Network derivative mining. In *Proceedings of the 28th ACM*
511 *International Conference on Information and Knowledge Management, CIKM '19*, page 861–870, New
512 York, NY, USA, 2019. Association for Computing Machinery. ISBN 9781450369763. doi: 10.1145/
513 3357384.3357910. URL <https://doi.org/10.1145/3357384.3357910>. 7, 18
- 514 [46] Franco P Preparata and Michael I Shamos. *Computational geometry: an introduction*. Springer Science &
515 Business Media, 2012. URL <http://www.cs.kent.edu/~dragan/CG/CG-Book.pdf>. 8
- 516 [47] Joshua Batson, Daniel A. Spielman, Nikhil Srivastava, and Shang-Hua Teng. Spectral sparsification
517 of graphs: Theory and algorithms. *Commun. ACM*, 56(8):87–94, aug 2013. ISSN 0001-0782. doi:
518 10.1145/2492007.2492029. URL <https://doi.org/10.1145/2492007.2492029>. 15
- 519 [48] Morteza Alamgir and Ulrike Luxburg. Phase transition in the family of p-resistances. In *Advances*
520 *in Neural Information Processing Systems*, 2011. URL [https://proceedings.neurips.cc/paper/2011/file/](https://proceedings.neurips.cc/paper/2011/file/07cdfd23373b17c6b337251c22b7ea57-Paper.pdf)
521 [07cdfd23373b17c6b337251c22b7ea57-Paper.pdf](https://proceedings.neurips.cc/paper/2011/file/07cdfd23373b17c6b337251c22b7ea57-Paper.pdf). 19
- 522 [49] Morteza Alamgir and Ulrike Luxburg. Phase transition in the family of p-resistances. In *Advances in*
523 *Neural Information Processing Systems*, volume 24, 2011. URL [https://proceedings.neurips.cc/paper/](https://proceedings.neurips.cc/paper/2011/file/07cdfd23373b17c6b337251c22b7ea57-Paper.pdf)
524 [2011/file/07cdfd23373b17c6b337251c22b7ea57-Paper.pdf](https://proceedings.neurips.cc/paper/2011/file/07cdfd23373b17c6b337251c22b7ea57-Paper.pdf). 19
- 525 [50] Gregory Berkolaiko, James B Kennedy, Pavel Kurasov, and Delio Mugnolo. Edge connectivity and the
526 spectral gap of combinatorial and quantum graphs. *Journal of Physics A: Mathematical and Theoretical*,
527 50(36):365201, 2017. URL <https://doi.org/10.1088/1751-8121/aa8125>. 19
- 528 [51] Zoran Stanić. Graphs with small spectral gap. *Electronic Journal of Linear Algebra*, 26:28, 2013. URL
529 <https://journals.uwo.edu/index.php/ela/article/view/1259>. 19

530 **A Appendix**

531 In Appendix A we include a Table with the notation used in the paper and we provide an analysis of
 532 the diffusion and its relationship with curvature. In Appendix B, we study in detail GAP-LAYER and
 533 the implications of the proposed spectral gradients. Appendix C reports statistics and characteristics of
 534 the datasets used in the experimental section, provides more information about the experiments results,
 535 describes additional experimental results, and includes a summary of the computing infrastructure
 used in our experiments.

Table 2: Notation.

Symbol	Description
$G = (V, E)$	Graph = (Nodes, Edges)
\mathbf{A}	Adjacency matrix: $\mathbf{A} \in \mathbb{R}^{n \times n}$
\mathbf{X}	Feature matrix: $\mathbf{X} \in \mathbb{R}^{n \times F}$
v	Node $v \in V$ or $u \in V$
e	Edge $e \in E$
x	Features of node v : $x \in X$
n	Number of nodes: $n = V $
F	Number of features
\mathbf{D}	Degree diagonal matrix where d_v in D_{vv}
d_v	Degree of node v
$vol(G)$	Sum of the degrees of the graph $vol(G) = Tr[D]$
\mathbf{L}	Laplacian: $\mathbf{L} = \mathbf{D} - \mathbf{A}$
\mathbf{B}	Signed edge-vertex incidence matrix
\mathbf{b}_e	Incidence vector: Row vector of \mathbf{B} , with $\mathbf{b}_{e=(u,v)} = (\mathbf{e}_u - \mathbf{e}_v)$
\mathbf{v}_e	Projected incidence vector: $\mathbf{v}_e = \mathbf{L}^{+1/2} \mathbf{b}_e$
Γ	Ratio $\Gamma = \frac{1+\epsilon}{1-\epsilon}$
\mathcal{E}	Dirichlet Energy wrt \mathbf{L} : $\mathcal{E}(\mathbf{x}) := \mathbf{x}^T \mathbf{L} \mathbf{x}$
\mathcal{L}	Normalized Laplacian: $\mathcal{L} = \mathbf{I} - \mathbf{D}^{-1/2} \mathbf{A} \mathbf{D}^{-1/2}$
Λ	Eigenvalue matrix of \mathbf{L}
Λ'	Eigenvalue matrix of \mathcal{L}
λ_i	i -th eigenvalue of \mathbf{L}
λ_2	Second eigenvalue of \mathbf{L} : Spectral gap
λ'_i	i -th eigenvalue of \mathcal{L}
λ'_2	Second eigenvalue of \mathcal{L} : Spectral gap
\mathbf{F}	Matrix of eigenvectors of \mathbf{L}
\mathbf{G}	Matrix of eigenvectors of \mathcal{L}
\mathbf{f}_i	i eigenvector of \mathbf{L}
\mathbf{f}_2	Second eigenvector of \mathbf{L} : Fiedler vector
\mathbf{g}_i	i eigenvector of \mathcal{L}
\mathbf{g}_2	Second eigenvector of \mathcal{L} : Fiedler vector
$\tilde{\mathbf{A}}$	New Adjacency matrix
E'	New edges
H_{uv}	Hitting time between u and v
CT_{uv}	Commute time: $CT_{uv} = H_{uv} + H_{vu}$
R_{uv}	Effective resistance: $R_{uv} = CT_{uv}/vol(G)$
\mathbf{Z}	Matrix of commute times embeddings for all nodes in G
\mathbf{z}_u	Commute time embedding of node u
\mathbf{T}^{CT}	Resistance diffusion or commute times diffusion
$\mathbf{R}(\mathbf{Z})$	Pairwise Euclidean distance of embedding \mathbf{Z} divided by $vol(G)$
\mathbf{S}	Cluster assignment matrix: $\mathbf{S} \in \mathbb{R}^{n \times 2}$
\mathbf{T}^{GAP}	GAP diffusion
\mathbf{e}_u	Unit vector with unit value at u and 0 elsewhere
$\nabla_{\tilde{\mathbf{A}}} \lambda_2$	Gradient of λ_2 wrt $\tilde{\mathbf{A}}$
$[\nabla_{\tilde{\mathbf{A}}} \lambda_2]_{ij}$	Gradient of λ_2 wrt $\tilde{\mathbf{A}}_{uv}$
p_u	Node curvature: $p_u := 1 - \frac{1}{2} \sum_{u \sim v} R_{uv}$
κ_{uv}	Edge curvature: $\kappa_{uv} := 2(p_u + p_v)/R_{uv}$
\oplus	Concatenation

537 **A.1 Appendix A: CT-LAYER**

 538 **A.1.1 Notation**

539 The Table 2 summarizes the notation used in the paper.

 540 **A.1.2 Analysis of Commute Times rewiring**

541 First, we provide an answer to the following question:

 542 *Is resistance diffusion via \mathbf{T}^{CT} a principled way of preserving the Cheeger constant?*

 543 We answer the question above by linking Theorems 1 and 2 in the paper with the Lovász bound.
 544 The outline of our explanation follows three steps.

- 545 • **Proposition 1: Theorem 1 (Sparsification)** provides a principled way to bias the adjacency
 546 matrix so that the edges with the largest weights in the rewired graph correspond to the edges in
 547 graph's bottleneck.
- 548 • **Proposition 2: Theorem 2 (Cheeger vs Resistance)** can be used to demonstrate that increasing
 549 the effective resistance leads to a mild reduction of the Cheeger constant.
- 550 • **Proposition 3: (Conclusion)** The effectiveness of the above theorems to contain the Cheeger
 551 constant is constrained by the Lovász bound.

552 Next, we provide a thorough explanation of each of the propositions above.

 553 **Proposition 1 (Biasing).** *Let $G' = \text{Sparsify}(G, q)$ be a sampling algorithm of graph $G = (V, E)$,
 554 where edges $e \in E$ are sampled with probability $q \propto R_e$ (proportional to the effective resistance).
 555 This choice is necessary to retain the global structure of G , i.e., to satisfy*

$$\forall \mathbf{x} \in \mathbb{R}^n : (1 - \epsilon) \mathbf{x}^T \mathbf{L}_G \mathbf{x} \leq \mathbf{x}^T \mathbf{L}_{G'} \mathbf{x} \leq (1 + \epsilon) \mathbf{x}^T \mathbf{L}_G \mathbf{x}, \quad (9)$$

 556 *with probability at least 1/2 by sampling $O(n \log n / \epsilon^2)$ edges, with $1/\sqrt{n} < \epsilon \leq 1$, instead of
 557 $O(m)$, where $m = |E|$. In addition, this choice biases the uniform distribution in favor of critical
 558 edges in the graph.*

 559 *Proof.* We start by expressing the Laplacian \mathbf{L} in terms of the edge-vertex incidence matrix $\mathbf{B}_{m \times e}$:

$$\mathbf{B}_{eu} = \begin{cases} 1 & \text{if } u \text{ is the head of } e \\ -1 & \text{if } u \text{ is the tail of } e \\ 0 & \text{otherwise.} \end{cases} \quad (10)$$

 560 where edges in undirected graphs are counted once, i.e. $e = (u, v) = (v, u)$. Then, we have
 561 $\mathbf{L} = \mathbf{B}^T \mathbf{B} = \sum_e \mathbf{b}_e \mathbf{b}_e^T$, where \mathbf{b}_e is a row vector (*incidence vector*) of \mathbf{B} , with $\mathbf{b}_{e=(u,v)} = (\mathbf{e}_u - \mathbf{e}_v)$.
 562 In addition, the Dirichlet energies can be expressed as norms:

$$\mathcal{E}(\mathbf{x}) = \mathbf{x}^T \mathbf{L} \mathbf{x} = \mathbf{x}^T \mathbf{B}^T \mathbf{B} \mathbf{x} = \|\mathbf{B} \mathbf{x}\|_2^2 = \sum_{e=(u,v) \in E} (\mathbf{x}_u - \mathbf{x}_v)^2. \quad (11)$$

 563 As a result, the effective resistance R_e between the two nodes of an edge $e = (u, v)$ can be defined as

$$R_e = (\mathbf{e}_u - \mathbf{e}_v)^T \mathbf{L}^+ (\mathbf{e}_u - \mathbf{e}_v) = \mathbf{b}_e^T \mathbf{L}^+ \mathbf{b}_e \quad (12)$$

 565 Next, we reformulate the spectral constraints in Eq. 9, i.e. $(1 - \epsilon) \mathbf{L}_G \preceq \mathbf{L}_{G'} \preceq (1 + \epsilon) \mathbf{L}_G$ as

$$\mathbf{L}_G \preceq \mathbf{L}_{G'} \preceq \Gamma \mathbf{L}_G, \Gamma = \frac{1 + \epsilon}{1 - \epsilon}. \quad (13)$$

 566 This simplifies the analysis, since the above expression can be interpreted as follows: the Dirichlet
 567 energies of $\mathbf{L}_{G'}$ are lower-bounded by those of \mathbf{L}_G and upper-bounded by Γ times the energies of
 568 \mathbf{L}_G . Considering that the energies define hyper-ellipsoids, the hyper-ellipsoid associated with $\mathbf{L}_{G'}$ is
 569 between the hyper-ellipsoids of \mathbf{L}_G and Γ times the \mathbf{L}_G .

 570 The hyper-ellipsoid analogy provides a framework to proof that the inclusion relationships are
 571 preserved under scaling: $M \mathbf{L}_G M \preceq M \mathbf{L}_{G'} M \preceq M \Gamma \mathbf{L}_G M$ where M can be a matrix. In this case,
 572 if we set $M := (\mathbf{L}_G^+)^{1/2} = \mathbf{L}_G^{+1/2}$ we have:

$$\mathbf{L}_G^{+1/2} \mathbf{L}_G \mathbf{L}_G^{+1/2} \preceq \mathbf{L}_G^{+1/2} \mathbf{L}_{G'} \mathbf{L}_G^{+1/2} \preceq \mathbf{L}_G^{+1/2} \Gamma \mathbf{L}_G \mathbf{L}_G^{+1/2}, \quad (14)$$

573 which leads to

$$\mathbf{I}_n \preceq \mathbf{L}_G^{+/2} \mathbf{L}_{G'} \mathbf{L}_G^{+/2} \preceq \Gamma \mathbf{I}_n . \quad (15)$$

574 We seek a Laplacian $\mathbf{L}_{G'}$ satisfying the *similarity constraints* in Eq. 13. Since $E' \subset E$, i.e. we want
575 to remove structurally irrelevant edges, we can design $\mathbf{L}_{G'}$ in terms of considering *all* the edges E :

$$\mathbf{L}_{G'} := \mathbf{B}_G^T \mathbf{B}_G = \sum_e s_e \mathbf{b}_e \mathbf{b}_e^T \quad (16)$$

576 and let the similarity constraint define the sampling weights and the choice of e (setting $s_e \geq 0$
577 properly). More precisely:

$$\mathbf{I}_n \preceq \mathbf{L}_G^{+/2} \sum_e \mathbf{b}_e \mathbf{b}_e^T \mathbf{L}_G^{+/2} \preceq \Gamma \mathbf{I}_n . \quad (17)$$

578 Then if we define $\mathbf{v}_e := \mathbf{L}_G^{+/2} \mathbf{b}_e$ as the *projected incidence vector*, we have

$$\mathbf{I}_n \preceq \sum_e s_e \mathbf{v}_e \mathbf{v}_e^T \preceq \Gamma \mathbf{I}_n . \quad (18)$$

579 Consequently, a spectral sparsifier must find $s_e \geq 0$ so that the above similarity constraint is satisfied.
580 Since there are m edges in E , s_e must be zero for most of the edges. But, what are the best candidates
581 to retain? Interestingly, the similarity constraint provides the answer. From Eq. 12 we have

$$\mathbf{v}_e^T \mathbf{v}_e = \|\mathbf{v}_e\|^2 = \|\mathbf{L}_G^{+/2} \mathbf{b}_e\|_2^2 = \mathbf{b}_e^T \mathbf{L}_G^+ \mathbf{b}_e = R_e . \quad (19)$$

582 This result explains why sampling the edges with probability $q \propto R_e$ leads to a ranking of m edges
583 of $G = (V, E)$ such that edges with large $R_e = \|\mathbf{v}_e\|^2$ are preferred³.

584 Algorithm 1 implements a deterministic greedy version of $\text{Sparsify}(G, q)$, where we build incremen-
585 tally $E' \subset E$ by creating a budget of decreasing resistances $R_{e_1} \geq R_{e_2} \geq \dots \geq R_{e_{O(n \log n / \epsilon^2)}}$. \square

586 Note that this rewiring strategy preserves the spectral similarities of the graphs, i.e. the global
587 structure of $G = (V, E)$ is captured by $G' = (V, E')$.

588 Moreover, the maximum R_e in each graph determines an upper bound on the Cheeger constant and
589 hence an upper bound on the size of the graph's bottleneck, as per the following proposition.

Algorithm 1: GREEDYSparsify

Input : $G = (V, E), \epsilon \in (1/\sqrt{n}, 1], n = |V|$.

Output : $G' = (V, E')$ with $E' \subset E$ such that $|E'| = O(n \log n / \epsilon^2)$.

$L \leftarrow \text{List}(\{\mathbf{v}_e : e \in E\})$

$Q \leftarrow \text{Sort}(L, \text{descending, criterion}=\|\mathbf{v}_e\|^2)$ \triangleright Sort candidate edges by descending Resistance

$E' \leftarrow \emptyset$

$\mathcal{I} \leftarrow \mathbf{0}_{n \times n}$

repeat

$\mathbf{v}_e \leftarrow \text{pop}(Q)$ \triangleright Remove the head of the queue

$\mathcal{I} \leftarrow \mathcal{I} + \mathbf{v}_e \mathbf{v}_e^T$

if $\mathcal{I} \preceq \Gamma \mathbf{I}_n$ **then**

$E' \leftarrow E' \cup \{e\}$

\triangleright Update the current budget of edges

else

return $G' = (V, E')$

until $Q = \emptyset$

590 **Proposition 2** (Resistance Diameter). *Let $G' = \text{Sparsify}(G, q)$ be a sampling algorithm of graph*
591 *$G = (V, E)$, where edges $e \in E$ are sampled with probability $q \propto R_e$ (proportional to the effective*
592 *resistance). Consider the resistance diameter $\mathcal{R}_{diam} := \max_{u,v} R_{uv}$. Then, for the pair of (u, v)*

³Although some of the elements of this section are derived from [47], we note that the Nikhil Srivastava's lectures at The Simons Institute (2014) are by far more clarifying.

593 does exist an edge $e = (u, v) \in E'$ in $G' = (V, E')$ such that $R_e = \mathcal{R}_{diam}$. As a result the Cheeger
 594 constant of G h_G is upper-bounded as follows:

$$h_G \leq \frac{\alpha^\epsilon}{\sqrt{\mathcal{R}_{diam} \cdot \epsilon}} \text{vol}(S)^{\epsilon-1/2}, \quad (20)$$

595 with $0 < \epsilon < 1/2$ and $d_u \geq 1/\alpha$ for all $u \in V$.

596 *Proof.* The fact that the maximum resistance \mathcal{R}_{diam} is located in an edge is derived from two
 597 observations: a) Resistance is upper bounded by the shortest-path distance; and b) edges with
 598 maximal resistance are prioritized in (Proposition 1).

599 Theorem 2 states that any attempt to increase the graph's bottleneck in a multiplicative way (i.e.
 600 multiplying it by a constant $c \geq 0$) results in decreasing the effective resistances as follows:

$$R_{uv} \leq \left(\frac{1}{d_u^{2\epsilon}} + \frac{1}{d_v^{2\epsilon}} \right) \cdot \frac{1}{\epsilon \cdot c^2} \quad (21)$$

601 with $\epsilon \in [0, 1/2]$. This equation is called the *resistance bound*. Therefore, a multiplicative increase of
 602 the bottleneck leads to a quadratic decrease of the resistances.

603 Following Corollary 2 of [42], we obtain an upper bound of any h_S , i.e. the Cheeger constant for
 604 $S \subseteq V$ with $\text{vol}(S) \leq \text{vol}(G)/2$ – by defining c properly. In particular we are seeking a value of c
 605 that would lead to a contradiction, which is obtained by setting

$$c = \sqrt{\frac{\left(\frac{1}{d_{u^*}^{2\epsilon}} + \frac{1}{d_{v^*}^{2\epsilon}} \right)}{\mathcal{R}_{diam} \cdot \epsilon}}, \quad (22)$$

606 where (u^*, v^*) is a pair of nodes with maximal resistance, i.e. $R_{u^*v^*} = \mathcal{R}_{diam}$.

607 Consider now any other pair of nodes (s, t) with $R_{st} < \mathcal{R}_{diam}$. Following Theorem 2, if the
 608 bottleneck of h_S is multiplied by c , we should have

$$R_{st} \leq \left(\frac{1}{d_s^{2\epsilon}} + \frac{1}{d_t^{2\epsilon}} \right) \cdot \frac{1}{\epsilon \cdot c^2} = \left(\frac{1}{d_s^{2\epsilon}} + \frac{1}{d_t^{2\epsilon}} \right) \cdot \frac{\mathcal{R}_{diam}}{\left(\frac{1}{d_{u^*}^{2\epsilon}} + \frac{1}{d_{v^*}^{2\epsilon}} \right)}. \quad (23)$$

609 However, since $\mathcal{R}_{diam} \leq \left(\frac{1}{d_{u^*}^{2\epsilon}} + \frac{1}{d_{v^*}^{2\epsilon}} \right)$ we have that R_{st} can satisfy

$$R_{st} > \left(\frac{1}{d_s^{2\epsilon}} + \frac{1}{d_t^{2\epsilon}} \right) \cdot \frac{1}{\epsilon \cdot c^2} \quad (24)$$

610 which is a contradiction and enables

$$h_S \leq \frac{c}{\text{vol}(S)^{1/2-\epsilon}} \iff |\partial S| \leq c \cdot \text{vol}(S)^{1/2-\epsilon}. \quad (25)$$

611 Using c as defined in Eq. 22 and $d_u \geq 1/\alpha$ we obtain

$$c = \sqrt{\frac{\left(\frac{1}{d_{u^*}^{2\epsilon}} + \frac{1}{d_{v^*}^{2\epsilon}} \right)}{\mathcal{R}_{diam} \cdot \epsilon}} \leq \sqrt{\frac{\alpha^\epsilon}{\mathcal{R}_{diam} \cdot \epsilon}} \leq \frac{\alpha^\epsilon}{\sqrt{\mathcal{R}_{diam} \cdot \epsilon}}. \quad (26)$$

612 Therefore,

$$h_S \leq \frac{c}{\text{vol}(S)^{1/2-\epsilon}} \leq \frac{\alpha^\epsilon}{\sqrt{\mathcal{R}_{diam} \cdot \epsilon}} \cdot \frac{1}{\text{vol}(S)^{1/2-\epsilon}} = \frac{\alpha^\epsilon}{\sqrt{\mathcal{R}_{diam} \cdot \epsilon}} \cdot \text{vol}(S)^{\epsilon-1/2}. \quad (27)$$

613 As a result, the Cheeger constant of $G = (V, E)$ is mildly reduced (by the square root of the maximal
 614 resistance). \square

615 **Proposition 3** (Conclusion). *Let (u^*, v^*) be a pair of nodes (may be not unique) in $G = (V, E)$
 616 with maximal resistance, i.e. $R_{u^*v^*} = \mathcal{R}_{diam}$. Then, the Cheeger constant h_G relies on the ratio
 617 between the maximal resistance \mathcal{R}_{diam} and its uninformative approximation $\left(\frac{1}{d_{u^*}^{2\epsilon}} + \frac{1}{d_{v^*}^{2\epsilon}} \right)$. The closer
 618 this ratio is to the unit, the easier it is to contain the Cheeger constant.*

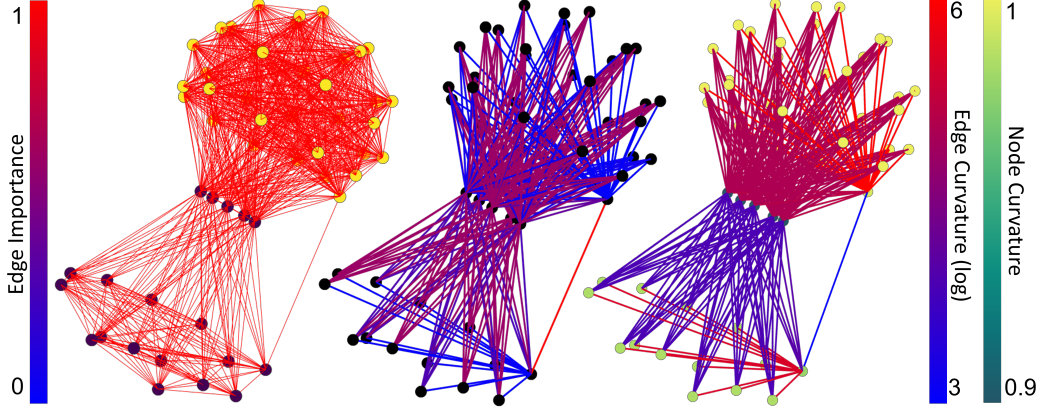


Figure 5: Left: Original graph with nodes colored as Louvain communities. Middle: \mathbf{T}^{CT} learnt by CT-LAYER with edges colors as node importance $[0,1]$. Right: Node and edge curvature: \mathbf{T}^{CT} using $p_u := 1 - \frac{1}{2} \sum_{u \sim w} \mathbf{T}_{uw}^{CT}$ and $\kappa_{uv} := 2(p_u + p_v) / \mathbf{T}_{uv}^{CT}$ with edge and node curvatures as color. Graph from Reddit-B dataset.

619 *Proof.* The referred ratio above is the ratio leading to a proper c in Proposition 2. This is consistent
 620 with a Lovász regime where the spectral gap λ_2' has a moderate value. However, for regimes with
 621 very small spectral gaps, i.e. $\lambda_2' \rightarrow 0$, according to the Lovász bound, $\mathcal{R}_{diam} \gg \left(\frac{1}{d_u^*} + \frac{1}{d_v^*}\right)$ and
 622 hence the Cheeger constant provided by Proposition 2 will tend to zero. \square

623 We conclude that we can always find an moderate upper bound for the Cheeger constant of $G =$
 624 (V, E) , provided that the regime of the Lovász bound is also moderate. Therefore, as the global
 625 properties of $G = (V, E)$ are captured by $G' = (V, E')$, a moderate Cheeger constant, when
 626 achievable, also controls the bottlenecks in $G' = (V, E')$.

627 Our methodology has focused on first exploring the properties of the commute times / effective
 628 resistances in $G = (V, E)$. Next, we have leveraged the spectral similarity to reason about the
 629 properties –particularly the Cheeger constant– of $G = (V, E')$. In sum, we conclude that resistance
 630 diffusion via \mathbf{T}^{CT} is a principled way of preserving the Cheeger constant of $G = (V, E)$.

631 A.1.3 Resistance-based Curvatures

632 We refer to recent work by Devriendt and Lambiotte [24] to complement the contributions of Topping
 633 et al. [20] regarding the use of curvature to rewire the edges in a graph.

634 **Theorem 3** (Devriendt and Lambiotte [24]). *The edge resistance curvature has the following prop-*
 635 *erties: (1) It is bounded by $(4 - d_u - d_v) \leq \kappa_{uv} \leq 2/R_{uv}$, with equality in the lower bound iff*
 636 *all incident edges to u and v are cut links; (2) It is upper-bounded by the Ollivier-Ricci curvature*
 637 *$\kappa_{uv}^{OR} \geq \kappa_{uv}$, with equality if (u, v) is a cut link; and (3) Forman-Ricci curvature is bounded as*
 638 *follows: $\kappa_{uv}^{FR}/R_{uv} \leq \kappa_{uv}$ with equality in the bound if the edge is a cut link.*

639 The new definition of curvature given in [20] is related to the resistance distance and thus it is
 640 learnable with the proposed framework (CT-LAYER). Actually, the Balanced-Forman curvature
 641 (Definition 1 in [20]) relies on the uniform approximation of the resistance distance.

642 Figure 5 illustrates the relationship between effective resistances / commute times and curvature on
 643 an exemplary graph from the COLLAB dataset.

644 As seen in the Figure, effective resistances prioritize the edges connecting outer nodes with hubs
 645 or central nodes, while the intra-community connections are de-prioritized. This observation is
 646 consistent with the aforementioned theoretical explanations about preserving the bottleneck while
 647 breaking the intra-cluster structure. In addition, we also observe that the original edges between hubs
 648 have been deleted or have been extremely down-weighted.

649 Regarding curvature, hubs or central nodes have the lowest node curvature (this curvature increases
 650 with the number of nodes in a cluster/community). Edge curvatures, which rely on node curvatures,
 651 depend on the long-term neighborhoods of the connecting nodes. In general, edge curvatures can be
 652 seen as a smoothed version –since they integrate node curvatures– of the inverse of the resistance
 653 distances.

654 We observe that edges linking nodes of a given community with hubs tend to have similar edge-
 655 curvature values. However, edges linking nodes of different communities with hubs have different
 656 edge curvatures (Figure 5-right). This is due to the different number of nodes belonging to each
 657 community, and to their different average degree inside their respective communities (property 1 of
 658 Theorem 3).

659 Finally, note that the range of edge curvatures is larger than that of resistance distances. The sparsifier
 660 transforms a uniform distribution of the edge weights into a less entropic one: in the example of
 661 Figure 5 we observe a power-law distribution of edge resistances. As a result, $\kappa_{uv} := 2(p_u + p_v) / \mathbf{T}_{uv}^{CT}$
 662 becomes very large on average (edges with infinite curvature are not shown in the plot) and a log
 663 scale is needed to appreciate the differences between edge resistances and edge curvatures.

664 A.2 Appendix B: GAP-LAYER

665 A.2.1 Spectral Gradients

666 The proposed GAP-LAYER relies on gradients wrt the Laplacian eigenvalues, and particularly the
 667 spectral gap (λ_2 for \mathbf{L} and λ'_2 wrt \mathcal{L}). Although the GAP-LAYER inductively rewires the adjacency
 668 matrix \mathbf{A} so that λ_2 is minimized, the gradients derived in this section may also be applied for gap
 669 maximization.

670 Note that while our cost function $L_{Fiedler} = \|\tilde{\mathbf{A}} - \mathbf{A}\|_F + \alpha(\lambda_2^*)^2$, with $\lambda_2^* \in \{\lambda_2, \lambda'_2\}$, relies on
 671 an eigenvalue, we *do not compute it explicitly*, as its computation has a complexity of $O(n^3)$ and
 672 would need to be computed in every learning iteration. Instead, we learn an approximation of λ_2 's
 673 eigenvector \mathbf{f}_2 and use its Dirchlet energy $\mathcal{E}(\mathbf{f}_2)$ to approximate the eigenvalue. In addition, since
 674 $\mathbf{g}_2 = \mathbf{D}^{1/2}\mathbf{f}_2$, we first approximate \mathbf{g}_2 and then approximate λ'_2 from $\mathcal{E}(\mathbf{g}_2)$.

675 **Gradients of the Ratio-cut Approximation.** Let \mathbf{A} be the adjacency matrix of $G = (V, E)$; and
 676 $\tilde{\mathbf{A}}$, a matrix similar to the original adjacency but with minimal λ_2 . Then, the gradient of λ_2 wrt each
 677 component of $\tilde{\mathbf{A}}$ is given by

$$\nabla_{\tilde{\mathbf{A}}} \lambda_2 := \text{Tr} \left[(\nabla_{\tilde{\mathbf{L}}} \lambda_2)^T \cdot \nabla_{\tilde{\mathbf{A}}} \tilde{\mathbf{L}} \right] = \text{diag}(\mathbf{f}_2 \mathbf{f}_2^T) \mathbf{1} \mathbf{1}^T - \mathbf{f}_2 \mathbf{f}_2^T, \quad (28)$$

678 where $\mathbf{1}$ is the vector of n ones; and $[\nabla_{\tilde{\mathbf{A}}} \lambda_2]_{ij}$ is the gradient of λ_2 wrt $\tilde{\mathbf{A}}_{uv}$. The above formula is
 679 an instance of the network derivative mining approach [45]. In this framework, λ_2 is seen
 680 as a function of $\tilde{\mathbf{A}}$ and $\nabla_{\tilde{\mathbf{A}}} \lambda_2$, the gradient of λ_2 wrt $\tilde{\mathbf{A}}$, comes from the chain rule of the matrix
 681 derivative $\text{Tr} \left[(\nabla_{\tilde{\mathbf{L}}} \lambda_2)^T \cdot \nabla_{\tilde{\mathbf{A}}} \tilde{\mathbf{L}} \right]$. More precisely,

$$\nabla_{\tilde{\mathbf{L}}} \lambda_2 := \frac{\partial \lambda_2}{\partial \tilde{\mathbf{L}}} = \mathbf{f}_2 \mathbf{f}_2^T, \quad (29)$$

682 is a matrix relying on an outer product (correlation). In the proposed GAP-LAYER, since \mathbf{f}_2 is
 683 approximated by:

$$\mathbf{f}_2(u) = \begin{cases} +1/\sqrt{n} & \text{if } u \text{ belongs to the first cluster} \\ -1/\sqrt{n} & \text{if } u \text{ belongs to the second cluster} \end{cases}, \quad (30)$$

684 i.e. we discard the $O\left(\frac{\log n}{n}\right)$ from Eq. 30 (the non-linearities conjectured in [17]) in order to simplify
 685 the analysis. After reordering the entries of \mathbf{f}_2 for the sake of clarity, $\mathbf{f}_2 \mathbf{f}_2^T$ is the following block
 686 matrix:

$$\mathbf{f}_2 \mathbf{f}_2^T = \left[\begin{array}{c|c} 1/n & -1/n \\ \hline -1/n & 1/n \end{array} \right] \text{ whose diagonal matrix is } \text{diag}(\mathbf{f}_2 \mathbf{f}_2^T) = \left[\begin{array}{c|c} 1/n & 0 \\ \hline 0 & 1/n \end{array} \right] \quad (31)$$

687 Then, we have

$$\nabla_{\tilde{\mathbf{A}}} \lambda_2 = \left[\begin{array}{c|c} 1/n & 1/n \\ \hline 1/n & 1/n \end{array} \right] - \left[\begin{array}{c|c} 1/n & -1/n \\ \hline -1/n & 1/n \end{array} \right] = \left[\begin{array}{c|c} 0 & 2/n \\ \hline 2/n & 0 \end{array} \right] \quad (32)$$

688 which explains the results in Figure 1-left: edges linking nodes belonging to the same cluster remain
 689 unchanged whereas inter-cluster edges have a gradient of $2/n$. This provides a simple explanation
 690 for $\mathbf{T}^{GAP} = \tilde{\mathbf{A}}(\mathbf{S}) \odot \mathbf{A}$. The additional masking added by the adjacency matrix ensures that we do
 691 not create new links.

692 **Gradients Normalized-cut Approximation.** Similarly, using λ'_2 for graph rewiring leads to the
 693 following complex expression:

$$\nabla_{\tilde{\mathbf{A}}} \lambda'_2 := \text{Tr} \left[(\nabla_{\tilde{\mathcal{L}}} \lambda_2)^T \cdot \nabla_{\tilde{\mathbf{A}}} \tilde{\mathcal{L}} \right] = \mathbf{d}' \left\{ \mathbf{g}_2^T \tilde{\mathbf{A}}^T \tilde{\mathbf{D}}^{-1/2} \mathbf{g}_2 \right\} \mathbf{1}^T + \mathbf{d}' \left\{ \mathbf{g}_2^T \tilde{\mathbf{A}} \tilde{\mathbf{D}}^{-1/2} \mathbf{g}_2 \right\} \mathbf{1}^T + \tilde{\mathbf{D}}^{-1/2} \mathbf{g}_2 \mathbf{g}_2^T \tilde{\mathbf{D}}^{-1/2}. \quad (33)$$

694 However, since $\mathbf{g}_2 = \mathbf{D}^{1/2} \mathbf{f}_2$ and $\mathbf{f}_2 = \mathbf{D}^{-1/2} \mathbf{g}_2$, the gradient may be simplified as follows:

$$\nabla_{\tilde{\mathbf{A}}} \lambda'_2 := \text{Tr} \left[(\nabla_{\tilde{\mathcal{L}}} \lambda_2)^T \cdot \nabla_{\tilde{\mathbf{A}}} \tilde{\mathcal{L}} \right] = \mathbf{d}' \left\{ \mathbf{f}_2^T \tilde{\mathbf{D}}^{1/2} \tilde{\mathbf{A}}^T \mathbf{f}_2 \right\} \mathbf{1}^T + \mathbf{d}' \left\{ \mathbf{f}_2^T \tilde{\mathbf{D}}^{1/2} \tilde{\mathbf{A}} \mathbf{f}_2 \right\} \mathbf{1}^T + \tilde{\mathbf{D}}^{-1/2} \mathbf{f}_2 \mathbf{f}_2^T \tilde{\mathbf{D}}^{-1/2}. \quad (34)$$

695 In addition, considering symmetry for the undirected graph case, we obtain:

$$\nabla_{\tilde{\mathbf{A}}} \lambda'_2 := \text{Tr} \left[(\nabla_{\tilde{\mathcal{L}}} \lambda_2)^T \cdot \nabla_{\tilde{\mathbf{A}}} \tilde{\mathcal{L}} \right] = 2\mathbf{d}' \left\{ \mathbf{f}_2^T \tilde{\mathbf{D}}^{1/2} \tilde{\mathbf{A}} \mathbf{f}_2 \right\} \mathbf{1}^T + \tilde{\mathbf{D}}^{-1/2} \mathbf{f}_2 \mathbf{f}_2^T \tilde{\mathbf{D}}^{-1/2}. \quad (35)$$

696 where \mathbf{d}' is a $n \times 1$ negative vector including derivatives of degree wrt adjacency and related terms.
 697 The obtained gradient is composed of two terms.

698 The first term contains the matrix $\tilde{\mathbf{D}}^{1/2} \tilde{\mathbf{A}}$ which is the adjacency matrix weighted by the square root
 699 of the degree; $\mathbf{f}_2^T \tilde{\mathbf{D}}^{1/2} \tilde{\mathbf{A}} \mathbf{f}_2$ is a quadratic form (similar to a Dirichlet energy for the Laplacian) which
 700 approximates an eigenvalue of $\tilde{\mathbf{D}}^{1/2} \tilde{\mathbf{A}}$. We plan to further analyze the properties of this term in
 701 future work.

702 The second term, $\tilde{\mathbf{D}}^{-1/2} \mathbf{f}_2 \mathbf{f}_2^T \tilde{\mathbf{D}}^{-1/2}$, downweights the correlation term for the Ratio-cut case $\mathbf{f}_2 \mathbf{f}_2^T$
 703 by the degrees as in the normalized Laplacian. This results in a normalization of the Fiedler vector:
 704 $-1/n$ becomes $-\sqrt{d_u d_v}/n$ at the uv entry and similarly for $1/n$, i.e. each entry contains the average
 705 degree assortativity.

706 A.2.2 Beyond the Lovász Bound: the von Luxburg et al. bound

707 The Lovász bound was later refined by von Luxburg et al. [38] via a new, tighter bound which replaces
 708 d_{min} by d_{min}^2 in Eq. 1. Given that $\lambda'_2 \in (0, 2]$, as the number of nodes in the graph ($n = |V|$) and
 709 the average degree increase, then $R_{uv} \approx 1/d_u + 1/d_v$. This is likely to happen in certain types of
 710 graphs, such as Gaussian similarity-graphs –graphs where two nodes are linked if the neg-exponential
 711 of the distances between the respective features of the nodes is large enough; ϵ -graphs –graphs where
 712 the Euclidean distances between the features in the nodes are $\leq \epsilon$; and k -NN graphs with large k wrt
 713 n . The authors report a linear collapse of R_{uv} with the density of the graph in scale-free networks,
 714 such as social network graphs, whereas a faster collapse of R_{uv} has been reported in community
 715 graphs –congruent graphs with Stochastic Block Models (SBMs) [43].

716 Given the importance of the effective resistance, R_{uv} , as a *global* measure of node similarity, the
 717 von Luxburg et al.’s refinement motivated the development of *robust effective resistances*, mostly in
 718 the form of p -resistances given by $R_{uv}^p = \arg \min_{\mathbf{f}} \left\{ \sum_{e \in E} r_e |f_e|^p \right\}$, where \mathbf{f} is a unit-flow injected
 719 in u and recovered in v ; and $r_e = 1/w_e$ with w_e being the edge’s weight [48]. For $p = 1$, R_{uv}^p
 720 corresponds to the shortest path; $p = 2$ results in the effective resistance; and $p \rightarrow \infty$ leads to
 721 the inverse of the unweighted u - v -mincut⁴. Note that the optimal p value depends on the type of
 722 graph [48] and p -resistances may be studied from the perspective of p -Laplacians [44, 49].

723 While R_{uv} could be unbounded by minimizing the spectral gap λ'_2 , this approach has received little
 724 attention in the literature of mathematical characterization of graphs with small spectral gaps [50][51],
 725 i.e., instead of tackling the daunting problem of explicitly minimizing the gap, researchers in this
 726 field have preferred to find graphs with small spectral gaps.

⁴The link between CTs and mincuts is leveraged in the paper as an essential element of our approach.

727 **A.3 Appendix C: Experiments**

728 In this section, we provide details about the graphs contained in each of the datasets used in our
 729 experiments, a detailed clarification about architectures and experiments, and, finally, report additional
 730 experimental results.

731 **A.3.1 Datasets statistics**

732 Table 3 depicts the number of nodes, edges, average degree, assortativity, number of triangles,
 733 transitivity and clustering coefficients (mean and standard deviation) of all the graphs contained in
 734 each of the benchmark datasets used in our experiments. As seen in the Table, the datasets are very
 735 diverse in their characteristics. In addition, we use two synthetic datasets with 2 classes: Erdős-Rényi
 736 with $p_1 \in [0.3, 0.5]$ and $p_2 \in [0.4, 0.8]$ and Stochastic block model (SBM) with parameters $p_1 = 0.8$,
 737 $p_2 = 0.5$, $q_1 \in [0.1, 0.15]$ and $q_2 \in [0.01, 0.1]$.

Table 3: Dataset statistics. Parenthesis in *Assortativity* column denotes number of complete graphs (assortativity is undefined).

	Nodes	Egdes	AVG Degree	Triangles	Transitivity	Clustering	Assortativity
REDDIT-B	429.6 \pm 554	497.7 \pm 622	2.33 \pm 0.3	24 \pm 41	0.01 \pm 0.02	0.04 \pm 0.06	-0.364 \pm 0.17 (0)
IMDB-B	19.7 \pm 10	96.5 \pm 105	8.88 \pm 5.0	391 \pm 868	0.77 \pm 0.15	0.94 \pm 0.03	-0.135 \pm 0.16 (139)
COLLAB	74.5 \pm 62	2457 \pm 6438	37.36 \pm 44	$12 \times 10^4 \pm 48 \times 10^4$	0.76 \pm 0.21	0.89 \pm 0.08	-0.033 \pm 0.24 (680)
MUTAG	2.2 \pm 0.1	19.8 \pm 5.6	2.18 \pm 0.1	0.00 \pm 0.0	0.00 \pm 0.00	0.00 \pm 0.00	-0.279 \pm 0.17 (0)
PROTEINS	39.1 \pm 45.8	72.8 \pm 84.6	3.73 \pm 0.4	27.4 \pm 30	0.48 \pm 0.20	0.51 \pm 0.23	-0.065 \pm 0.2 (13)

738 In addition, Figure 6 depicts the histograms of the assortativity for all the graphs in each of the
 739 eight datasets used in our experiments. As shown in Table 3 assortativity is undefined in complete
 740 graphs (constant degree, all degrees are the same). Assortativity is defined as the normalized degree
 741 correlation. If the graph is complete, then both correlation and its variance is 0, so assortativity will
 742 be 0/0.

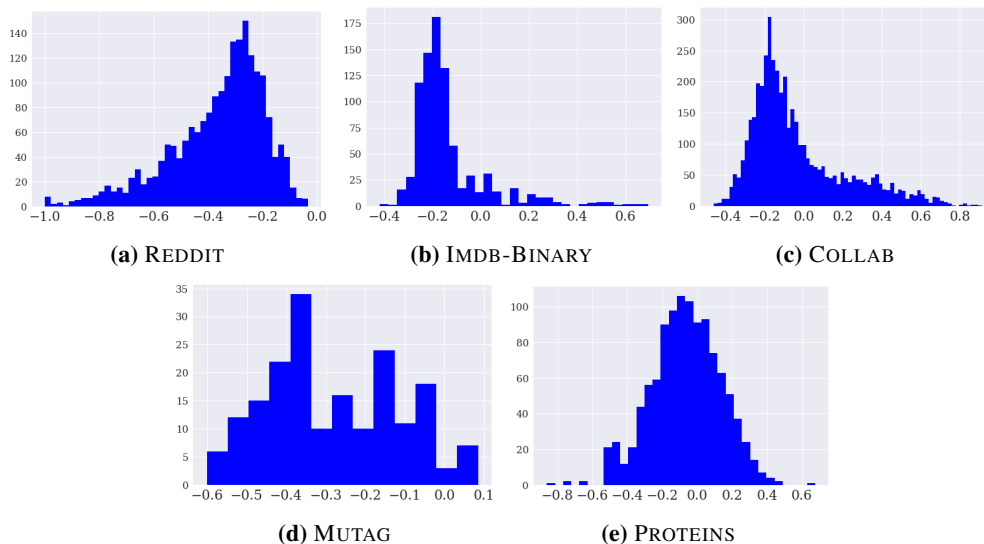


Figure 6: Histogram of the Assortativity of all the graphs in each of the datasets.

743 In addition, Figure 7 depicts the histograms of the average node degrees for all the graphs in each of
 744 the eight datasets used in our experiments. The datasets are also very diverse in terms of topology,
 745 corresponding to social networks, biochemical networks and meshes.

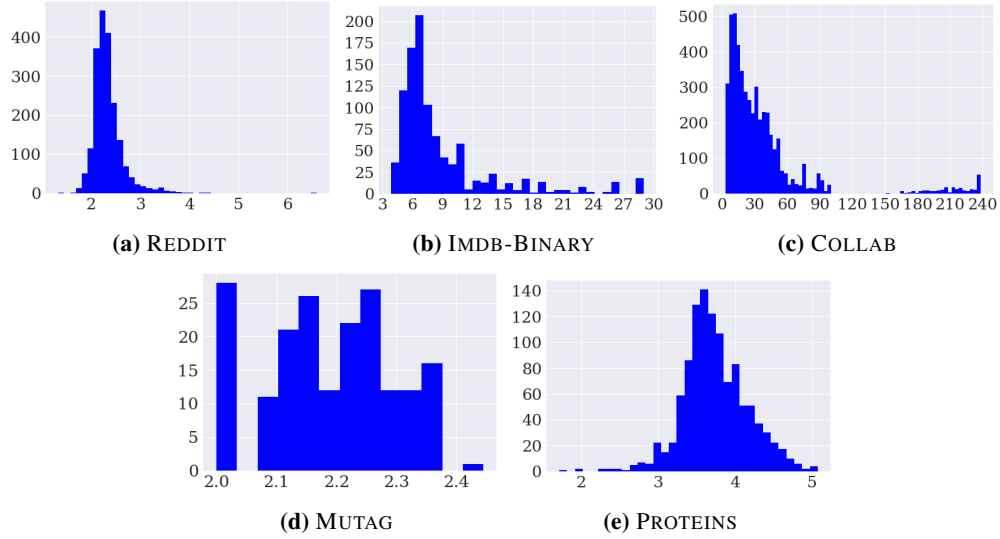


Figure 7: Degree histogram of the average degree of all the graphs in each of the datasets.

746 A.3.2 GNN architectures

747 Figure 8 shows the specific GNN architectures used in the experiments explained in section 4 in the
 748 manuscript. Although the specific calculation of \mathbf{T}^{GAP} and \mathbf{T}^{CT} are given in Theorems 2 and 1, we
 749 also provide a couple of pictures for a better intuition.

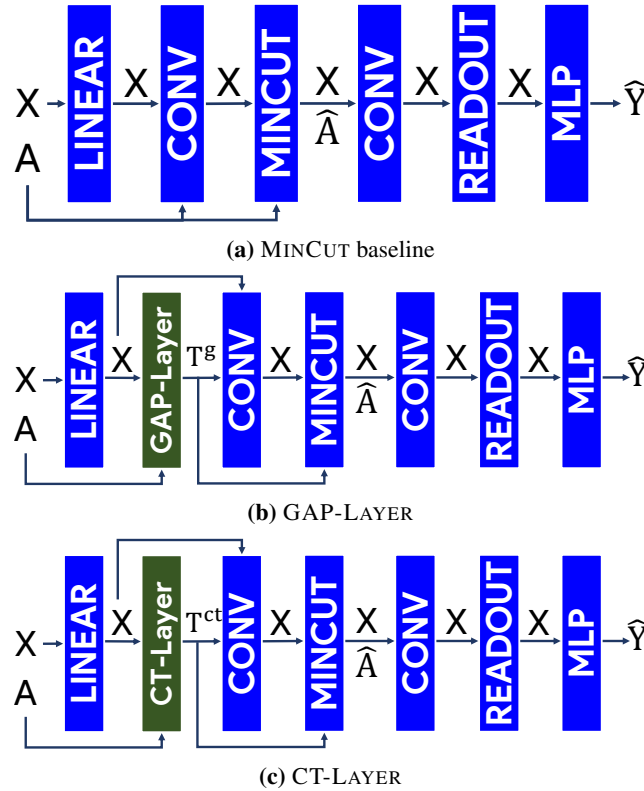


Figure 8: Diagrams of the GNNs used in the experiments.

750 A.3.3 Training parameters

751 The value of the hyperparameters used in the experiments are the ones by default in the anonymous
 752 repository ⁵. We report average accuracies and standard deviation on 10 random iterations, using
 753 different 85/15 train-test stratified split (we do not perform hyperparameter search), training during
 754 60 epochs and reporting the results of the last epoch for each random run. We have used an Adam
 755 optimizer, with a learning rate of $5e - 4$ and weight decay of $1e - 4$. In addition, the batch size
 756 used for the experiments are shown in Table 4. Regarding the synthetic datasets, the parameters are:
 757 Erdős-Rényi with $p_1 \in [0.3, 0.5]$ and $p_2 \in [0.4, 0.8]$ and Stochastic block model (SBM) $p_1 = 0.8$,
 758 $p_2 = 0.5$, $q_1 \in [0.1, 0.15]$ and $q_2 \in [0.01, 0.1]$.

Table 4: Dataset Batch size

	Batch	Dataset size
REDDIT-BINARY	64	1000
IMDB-BINARY	64	2000
COLLAB	64	5000
MUTAG	32	188
PROTEINS	64	1113
SBM	32	1000
Erdős-Rényi	32	1000

759 For the k -nn graph baseline, we choose k such that the main degree of the original graph is maintained,
 760 i.e. k equal to average degree. Our experiments also use 2 preprocessing methods DIGL and SDRF.
 761 Unlike our proposed methods, both SDRF [20] and DIGL [25] use a set of hyperparameters to
 762 optimize for each specific graph, because both are also not inductive. This approach could be
 763 manageable for the task of node classification, where you only have one graph. However, when it
 764 comes to graph classification, the number of graphs are huge (4) and it is nor computationally feasible
 765 optimize parameters for each specific graph. For DIGL, we use a fixed $\alpha = 0.001$ and ϵ based on
 766 keeping the same average degree for each graph, i.e., we use a different dynamically chosen ϵ for
 767 each graph in each dataset which maintain the same number of edges as the original graph. In the
 768 case of SDRF, the parameters define how stochastic the edge addition is (τ), the graph edit distance
 769 upper bound (number of iterations) and optional Ricci upper-bound above which an edge will be
 770 removed each iteration (C^+). We set the parameters $\tau = 20$ (the edge added is always near the edge
 771 of lower curvature), $C^+ = 0$ (to force one edge is removed every iteration), and number of iterations
 772 dynamic according to $0.7 * |V|$. Thus, we maintain the same number of edges in the new graph
 773 ($\tau = 20$ and $C^+ = 0$), i.e., same average degree, and we keep the graph distance to the original
 774 bounded by $0.7 * |V|$.

775 A.3.4 Latent Space Analysis

776 In this section, we analyze the two latent spaces produced by the models.

- 777 • First, we compare the CT Embedding computed spectrally (\mathbf{Z} in equation 2) with the CT
 778 Embedding predicted by our CT-LAYER (\mathbf{Z} in definition 1) for a given graph, where each point
 779 is a node in the graph.
- 780 • Second, we compare the graph readout output for every model defined in the experiments
 781 (Figure 4) where each point is a graph in the dataset.

782 **Spectral CT Embedding vs CT Embeddings Learned by CT-LAYER .** The well-known em-
 783 beddings based on the Laplacian positional encodings (PE) are typically computed beforehand and
 784 appended to the input vector \mathbf{X} as additional features [35, 36]. This task requires an expensive
 785 computation $O(n^3)$ (see equation 2). Conversely, we propose a GNN Layer that learns how to predict
 786 the CT embeddings (CTEs) for unseen graphs (definition 1 and Figure 2) with a loss function that
 787 optimizes such CTEs. Note that we do not explicitly use the CTE features (PE) for the nodes, but we
 788 use the CTs as a new diffusion matrix for message passing (given by \mathbf{T}^{CT} in Definition 1). Note that
 789 we could also use \mathbf{Z} as positional encodings in the node features, such that CT-LAYER may be seen
 790 as a novel approach to learn Positional Encodings.

⁵<https://anonymous.4open.science/r/DiffWireLoG22/readme.md>

791 In this section, we perform a comparative analysis between the spectral commute times embeddings
 792 (spectral CTEs, \mathbf{Z} in equation 2) and the CTEs that are predicted by our CT-LAYER (\mathbf{Z} in definition 1).
 793 As seen in Figure 9 (top), both embeddings respect the original topology of the graph, but they differ
 794 due to (1) orthogonality restrictions, and more interestingly to (2) the simplification of the original
 795 spectral loss function in Alev et al. [42]: the spectral CTEs minimize the trace of a quotient, which
 796 involves computing an inverse, whereas the CTEs learned in CT-LAYER minimize the quotient of
 797 two traces which is computationally simpler (see L_{CT} loss in Definition 1). Two important properties
 798 of the first term in Definition 1 are: (1) the learned embedding \mathbf{Z} has minimal Dirichlet energy
 799 (numerator) and (2) large degree nodes will be separated (denominator). Figure 9 (top) illustrates
 800 how the CTEs that are learned in CT-LAYER are able to better preserve the original topology of the
 801 graph (note how the nodes are more compactly embedded when compared to the spectral CTEs).

802 Figure 9 (bottom) depicts a histogram of the effective resistances or commute times (CTs) (see
 803 Section 3.2 in the paper) of the edges according to CT-LAYER or the spectral CTEs. The histogram is
 804 computed from the upper triangle of the \mathbf{T}^{CT} matrix defined in Definition 1. Note that the larger the
 805 effective resistance of an edge, the more important that edge will be considered (and hence the lower
 806 the probability of being removed [40]). We observe how in the histogram of CTEs that are learned
 807 in CT-LAYER there is a ‘small club’ of edges with very large values and a large number of edges
 808 with low values yielding a power-law-like profile. However, the histogram of the effective resistances
 809 computed by the spectral CTEs exhibits a profile similar to a Gaussian distribution. From this result,
 810 we conclude that the use of L_{CT} in the learning process of the CT-LAYER shifts the distribution of
 811 the effective resistances of the edges towards an asymmetric distribution where few edges have very
 812 large weights and a majority of edges have low weights.

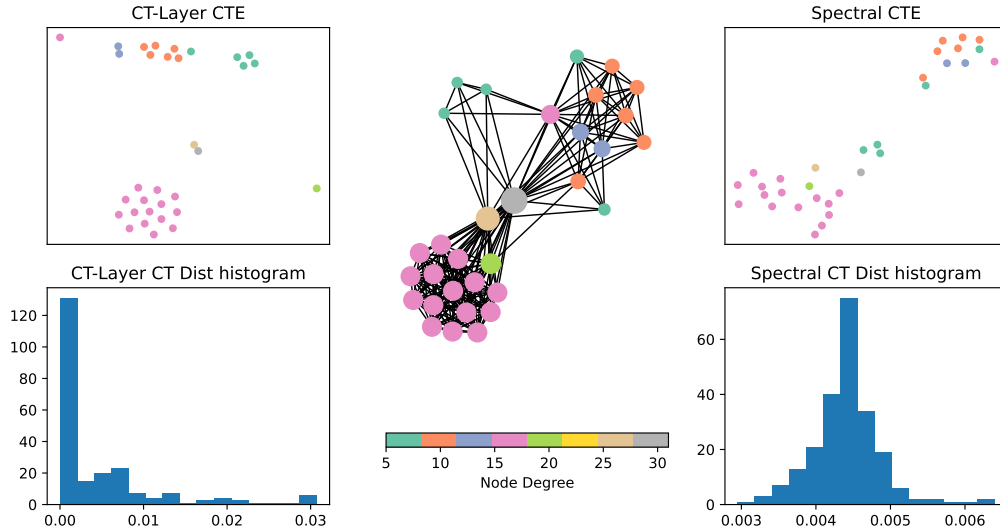


Figure 9: Top: CT embeddings predicted by CT-LAYER (left) and spectral CT embeddings (right). Bottom: Histogram of normalized effective resistances (i.e., CT distances or upper triangle in \mathbf{T}^{CT}) computed from the above CT embeddings. Middle: original graph from the COLLAB dataset. Colors correspond to node degree. CT-LAYER CTEs reduced from 75 to 32 dimensions using Johnson-Lindenstrauss. Finally, both CTEs reduced from 32 to 2 dimensions using T-SNE.

813 **Graph Readout Latent Space Analysis.** To delve into the analysis of the latent spaces produced
 814 by our layers and model, we also inspect the latent space produced by the models (Figure 4) that use
 815 MINCUTPOOL (Figure 8a), GAP-LAYER (Figure 8b) and CT-LAYER (Figure 8c). Each point is a
 816 graph in the dataset, corresponding to the graph embedding of the readout layer. We plot the output
 817 of the readout layer for each model, and then perform dimensionality reduction with TSNE.

818 Observing the latent space of the REDDIT-BINARY dataset (Figure 10), CT-LAYER creates a disperse
 819 yet structured latent space for the embeddings of the graphs. This topology in latent spaces show that
 820 this method is able to capture different topological details. The main reason is the expressiveness of
 821 the commute times as a distance metric when performing rewiring, which has been shown to be a

822 optimal metric to measure node structural similarity. In addition, GAP-LAYER creates a latent space
 823 where, although the 2 classes are also separable, the embeddings are more compressed, due to a more
 824 aggressive –yet still informative– change in topology. This change in topology is due to the change in
 825 bottleneck size that GAP-LAYER applies to the graph. Finally, MINCUT creates a more squeezed
 826 and compressed embedding, where both classes lie in the same spaces and most of the graphs have
 827 collapsed representations, due to the limited expressiveness of this architecture.

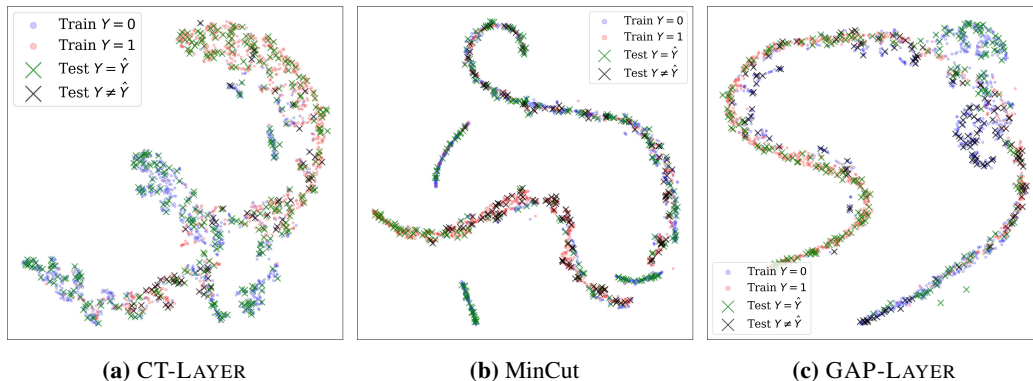


Figure 10: REDDIT embeddings produced by GAP-LAYER (Ncut) CT-LAYER and MINCUT.

828 A.3.5 Experiments in node classification with CT-LAYER

829 Although the contributions of this work are mainly designed for graph classification tasks, the
 830 applications in node classification are quite promising. We identify two potential areas to apply
 831 CT-LAYER in node classification.

832 First, the new \mathbf{T}^{CT} diffusion matrix learned by CT-LAYER gives larger weights (CTs or effective
 833 resistances) to edges that connect different communities, i.e., edges that connect distant nodes in
 834 the graph. This behaviour of CT-LAYER is aligned to solve long-range and heterophilic node
 835 classification tasks using fewer number of layers, avoiding under-reaching, over-smoothing and
 836 over-squashing. CT-LAYER will prioritize edges connecting distant nodes and thus with different
 837 labels.

838 Second, there is an increasingly interest in the community in using positional encodings (PEs) in the
 839 nodes for developing more expressive GNN. These PEs are features added to the node describing the
 840 local and global structural position and role of the node in the graph [34, 36]. PEs mainly help in
 841 node classification in homophilic graphs, as nearby nodes will be assigned similar PEs. Within the
 842 variety of measures used as PE (e.g. shortest paths, random walk probabilities, eigenvectors of the
 843 Laplacian. . .) commute times is one of the most expressive due to its spectral properties e.g. relation
 844 with the shortest path, spectral gap or Cheeger constant. The recent work by Velingker et al. [35]
 845 propose to append the commute times embedding (*resistive embeddings* in his work) to node features
 846 to improve the structural expressiveness of the GNN. However, the main limitation is that PEs are
 847 usually pre-computed and appended to \mathbf{X} before the GNN training due to its high computational
 848 cost. In this second area, CT-LAYER gives a solution to this problem. The proposed CT-LAYER also
 849 learns to predict the commute time embedding of a given graph (\mathbf{Z}) as part of the \mathbf{T}^{CT} computation
 850 (see Figure 2 and definition 1), and, hence, it can be seen as the first method that is able to learn and
 851 predict efficient PEs inside a GNN without need of pre-computing them.

852 However, the application of our framework for a node classification task entails several considerations.
 853 First, our implementation works with dense \mathbf{A} and \mathbf{X} matrices, whereas node classification typically
 854 uses sparse representations of the edges. Thus, the implementation of our proposed layers is not
 855 straightforward for sparse graph representations. Second, we anticipate a different behavior of our
 856 approach depending on the nature of the graphs: CT-LAYER should perform well in heterophilic
 857 graphs as the CTs (i.e. effective resistances) are larger in edges that connect different communities.
 858 However, it is not clear how well it would perform in homophilic graphs.

859 To shed light on the properties of each of the proposed methods, we perform a node classification
 860 task on well known homophilic and heterophilic graphs. The main purposes of this experiment are:

1) show the performance of CT-LAYER in heterophilic graphs using \mathbf{T}^{CT} as a matrix for message passing, and 2) show the ability of CT-LAYER to predict the commute times embedding and use it as a PE feature [35]. The results depicted in Table 5 summarizes the experimental results of node classification using 2 models. The first, CT embeddings (CTEs) as feature (\mathbf{Z} concatenated to \mathbf{X}) and, second, \mathbf{T}^{CT} as \mathbf{A} . Note that we have chosen benchmark datasets that are manageable with our dense implementation. In addition, we have chosen a basic baseline with 1 GCN layer to show the ability of the approaches to avoid under-reaching, over-smoothing and over-squashing.

Table 5: Results in node classification

Dataset	GCN	CT-LAYER ($\mathbf{X} \oplus \mathbf{Z}$)	CT-LAYER ($\mathbf{A} = \mathbf{T}^{\text{CT}}$)	Homophily
Cora	82.01 \pm 0.8	83.66\pm0.6	67.96 \pm 0.8	81.0%
Pubmed	81.61 \pm 0.3	86.07\pm0.1	68.19 \pm 0.7	80.0%
Citeseer	70.81 \pm 0.5	72.26\pm0.5	66.71 \pm 0.6	73.6%
Cornell	59.19 \pm 3.5	58.02 \pm 3.7	69.04\pm2.2	30.5%
Actor	29.59 \pm 0.4	29.35 \pm 0.4	31.98\pm0.3	21.9%
Wisconsin	68.05 \pm 6.2	69.25 \pm 5.1	79.05\pm2.1	19.6%

The baseline GCN is a 1-layer-GCN, and the 2 compared models are:

- 1 CT-LAYER for calculating \mathbf{Z} followed by 1 GCN Layer using that \mathbf{A} for message passing and $\mathbf{X} \oplus \mathbf{Z}$ as features. This approach is a combination of Vellingker et al. [35] and our method. See Figure 11b.
- 1 CT-LAYER for calculating \mathbf{T}^{CT} followed by 1 GCN Layer using that \mathbf{T}^{CT} for message passing and \mathbf{X} as features. See Figure 11c.

As expected, CTE as features performs well in heterophilic graphs and \mathbf{T}^{CT} as a diffusion matrix performs well in heterophilic graphs. Note that in our experiments the CTEs are learned by the CT-LAYER instead of being precomputed as in Vellingker et al. [35]. A promising direction of future work would be to explore how to combine both approaches to leverage the best of each of the methods on a wide range of graphs for node classification tasks.

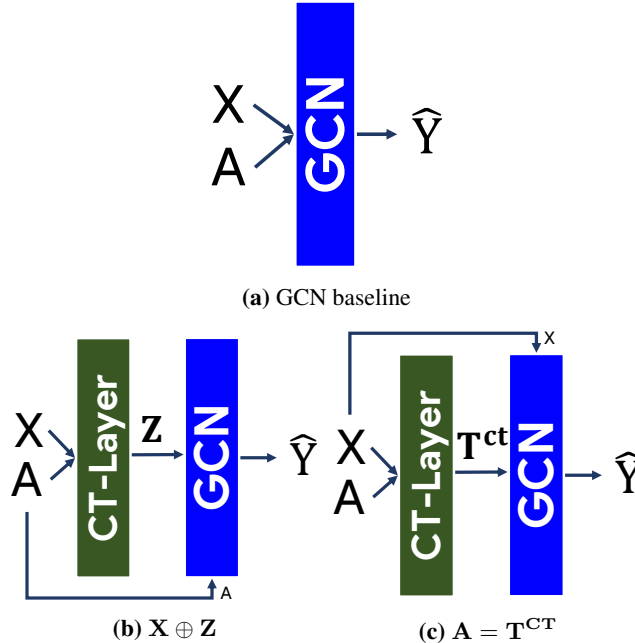


Figure 11: Diagrams of the GNNs used in the experiments for node classification.

879 **A.3.6 Analysis of correlation between structural properties and CT-LAYER performance**

880 To analyze the performance of our model in graphs with different structural properties, we analyze the
 881 correlation between accuracy, the graph’s assortativity, and the graph’s bottleneck (λ_2) in COLLAB
 882 and REDDIT datasets. If the error is consistent along all levels of accuracy and gaps, the layer can
 883 generalize along different graph topologies.

884 As seen in Figure 14, Figure 12 (middle), and Figure 13 (middle), we do not identify any correlation
 885 or systematic pattern between graph classification accuracy, assortativity, and bottleneck with CT-
 886 LAYER-based rewiring, since the proportion of wrong and correct predictions are regular for all levels
 887 of assortativity and bottleneck size.

888 In addition, note that while there is a systematic error of the model over-predicting class 0 in the
 889 COLLAB dataset (see Figure 12), this behavior is not explained by assortativity or bottleneck size,
 890 but by the unbalanced number of graphs in each class.

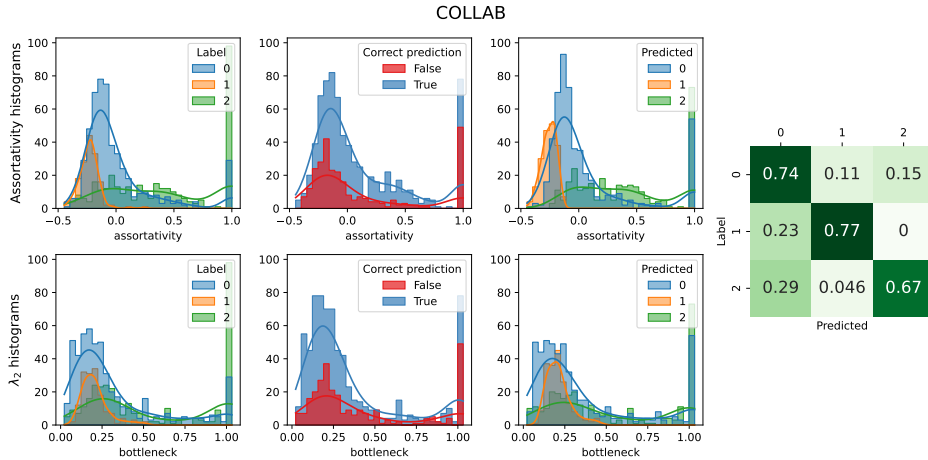


Figure 12: Analysis of assortativity, bottleneck and accuracy for COLLAB dataset. Top: Histograms of assortativity. Bottom: Histograms of bottleneck size (λ_2). Both are grouped by actual label of the graph (left), by correct or wrong predictions (middle) and by predicted label (right).

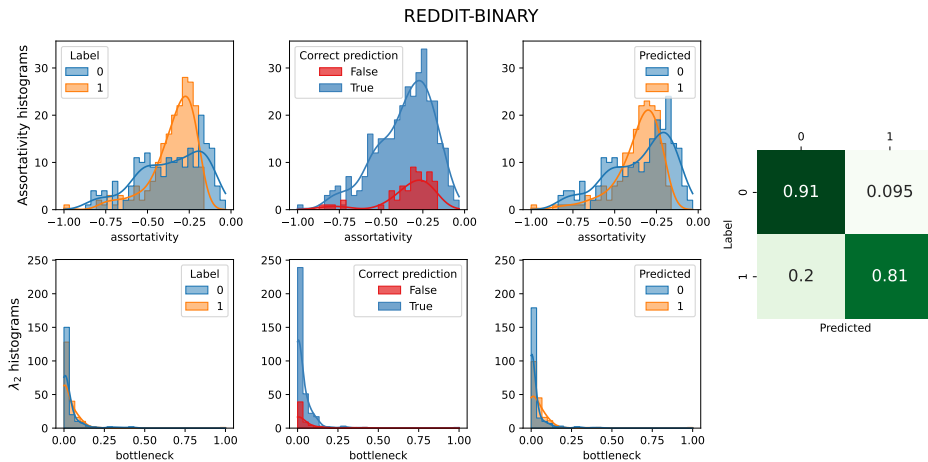


Figure 13: Analysis of assortativity, bottleneck and accuracy for REDDIT-B dataset. Top: Histograms of assortativity. Bottom: Histograms of bottleneck size (λ_2). Both are grouped by actual label of the graph (left), by correct or wrong predictions (middle) and by predicted label (right).

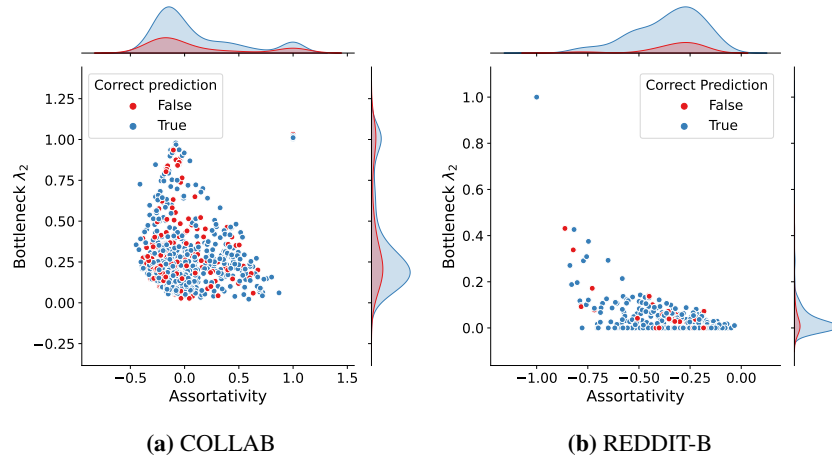


Figure 14: Correlation between assortativity, λ_2 and accuracy for CT-LAYER. Histograms shows that the proportion of correct and wrong predictions are regular for all levels of assortativity (x axis) and bottleneck size (y axis). For the sake of clarity, these visualizations, a and b, are the combination of the 2 histograms in the middle column of Figure 12 and Figure 13 respectively.

891 A.3.7 Computing infrastructure

892 Table 6 summarizes the computing infrastructure used in our experiments.

Table 6: Computing infrastructure.

Component	Details
GPU	2x A100-SXM4-40GB
RAM	1 TiB
CPU	255x AMD 7742 64-Core @ 2.25 GHz
OS	Ubuntu 20.04.4 LTS